C-PROOF O_2 Processing Report

Lauryn Talbot

May 2026

Introduction

Dissolved oxygen observations collected by glider optodes require several post-processing steps before they can be considered quantitatively reliable. This document describes the delayed-mode processing methodology currently used by C-PROOF and the rationale behind each correction.

C-PROOF uses both the Aanderaa 4831 and JFE Advantech Rinko AROD-FT optodes requiring slightly different processing approaches because of their different response times. Raw dissolved oxygen concentrations ([O_2]) exhibit pronounced upcast/downcast asymmetry and underestimate the corrected oxygen concentration by up to 26% for 99% of valid observations (Figure 1a).

C-PROOF applies three basic steps to the oxygen concentration:

1. Corrects the [O_2] magnitude for salinity and pressure biases (Figure 1b)
2. Addresses the upcast/downcast asymmetry (Figure 1c)
3. Corrects the [O_2] magnitude caused by optode drift over time (Figure 1d)

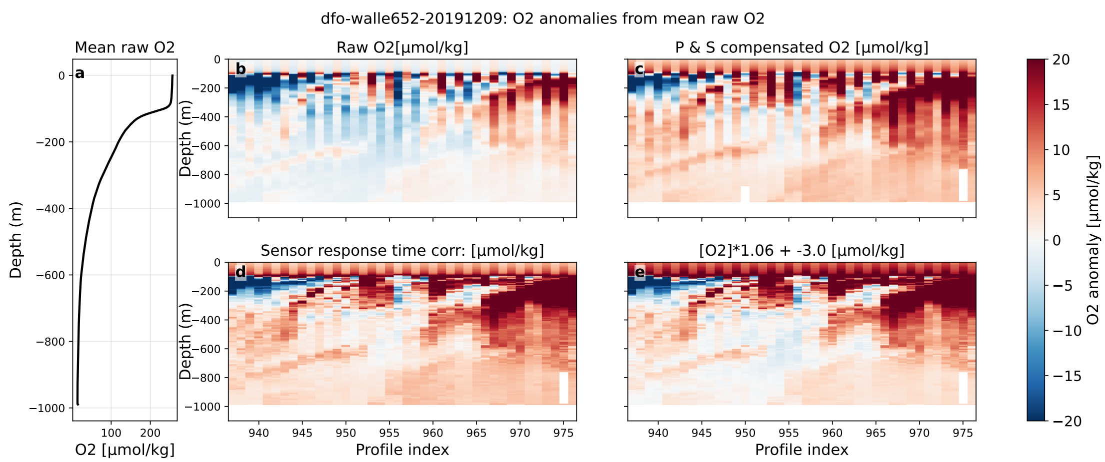

Figure 1: Example using dfo-walle652-20191209 with Aanderaa optode 4381: Anomaly of (b) Raw oxygen concentration ([O_2]) collected by the optode, (c) [O_2] accounting for pressure and salinity effects, (d) [O_2] from c) corrected for the sensor response time, (e) [O_2] from d) with a drift correction from the mean raw oxygen profile (a).

Specifications of both sensors is summarized in Table 1.

Parameter	Aanderaa 4831	Rinko ROD-FT
Resolution	$< 1\ \mu\text{mol}\,\text{L}^{-1}$	$1\ \mu\text{mol}\,\text{L}^{-1}$
Accuracy	Initial accuracy: $\pm 1.5\%$ of measured value or $\pm 2.0\ \mu\text{mol}\,\text{L}^{-1}$	Initial accuracy: $\pm 2\%$ of measured value or $\pm 2.0\ \mu\text{mol}\,\text{L}^{-1}$
	Long-term drift: $< 1\%$ per year	Sample-based drift: $< \pm 5\%$ of measured value or $\pm 5.0\ \mu\text{mol}\,\text{L}^{-1}$ per 4,000,000 samples
Response time	< 25 s	< 1 s in water
Measurement range	Oxygen concentration: 0–1000 $\mu\text{mol}\,\text{L}^{-1}$	Oxygen concentration: 0–425 $\mu\text{mol}\,\text{L}^{-1}$
	Air saturation: 0–300%	Air saturation: 0–200%

Table 1: Comparison of oxygen sensor specifications for the Aanderaa 4831 and Rinko AROD-FT optodes Aanderaa Data Instruments AS [2024], JFE Advantech Co., Ltd. [2023]

Contents

1 Optode descriptions

Aanderaa and Rinko optical oxygen sensors infer dissolved oxygen concentration by measuring how oxygen affects the behaviour of a luminophore porphyrin foil. The luminophore of both optodes sits within a sensing membrane or “indicator membrane” only penetrable by dissolved gases such as O_2, N_2 and water vapour [Bittig et al., 2018].The optode periodically illuminates the luminophore with blue light, exciting it to a higher energy state. As the luminophore relaxes back to its ground state, it emits red fluorescence. In the presence of dissolved oxygen, O_2 molecules collide with the excited luminophore and absorb part of its energy, a process known as quenching [Tengberg et al., 2006, Nicholson et al., 2008, Bittig et al., 2014]. Because quenching accelerates the return to the ground state, the emitted fluorescence decays more rapidly. The time required for the fluorescence intensity to decay, known as the fluorescence lifetime (τ), therefore decreases as oxygen concentration increases.

The luminescence intensity, I, and the fluorescence lifetime , τ are related through the Stern-Volmer equation to the partial pressure of oxygen present:

$$\frac{I_o}{I} = \frac{\tau_0}{\tau} = 1 + K_{SV} \cdot pO_2 \tag{1}$$

where pO_2 is the partial pressure of O_2 and K_{SV} is the Stern-Volmer constant (i.e. the quenching efficiency).

The equation can be simplified and pO_2 can be converted to [O_2]:

$$[O_2]_{uncompensated} = \frac{1}{K_{SV}}(\frac{\tau_o}{\tau} - 1) \tag{2}$$

2 Account for salinity and pressure effects

Aanderaa and Rinko sensors measure oxygen saturation (partial pressure) in water rather than dissolved oxygen concentration [Aanderaa Data Instruments AS, 2017]. Dissolved oxygen concentration is calculated from the measured pO_2, but this relationship depends on both seawater properties and sensor behaviour. Salinity changes the solubility of oxygen in seawater, so the same pO_2 can correspond to different dissolved oxygen concentrations. In addition, hydrostatic pressure alters the optode response by affecting the luminophore and oxygen quenching within the sensing foil. Therefore, both salinity and pressure corrections are required before converting the measured pO_2 to dissolved oxygen concentration.

A compensated oxygen in μmol/L is incorporating salinity and temperature effects is:

$$[O_{2,PS}] = [O_2]_{uncompented} \cdot s_{\text{factor}} \cdot p_{\text{factor}}$$

We call [O_2] corrected for pressure and salinity biases as [O_2,PS] in this report.

2.1 Salinity effect

Salinity reduces the absorption of O_2 in water, so the same pO_2 can result in different $[O_2]$ depending on the salinity of the water.

The salinity compensation factor is given by:

$$s_{\text{factor}} = \exp\left[(S - S_{\text{ref}})\left(B_0 + B_1 T_s + B_2 T_s^2 + B_3 T_s^3\right) + C_0\left(S^2 - S_{\text{ref}}^2\right)\right]$$

where

- S is the salinity collected from the glider CTD (PSU),
- S_{ref} is the internal reference salinity of the Aanderaa sensor (35 psu for C-PROOF Aanderaa sensors; 0 psu for C-PROOF Rinko AROD-RT sensors),
- B_0, B_1, B_2, B_3, and C_0 are empirical coefficients specified in the Aanderaa and Rinko calibration certificate from the manufacturer (Table 2),
- T_s is the scaled temperature defined as:

$$T_s = \ln\left(\frac{298.15 - T}{273.15 + T}\right)$$

- T is the in situ temperature from the CTD (°C).

Table 2: Salinity correction coefficients for the two optode models used by C-PROOF.

Coefficient	Aanderaa 4831	Rinko AROD-FT
B_0	-6.24097×10^{-3}	-6.24523×10^{-3}
B_1	-6.93498×10^{-3}	-7.37614×10^{-3}
B_2	-6.90358×10^{-3}	-1.03410×10^{-2}
B_3	-4.29155×10^{-3}	-8.17083×10^{-3}
C_0	-3.11680×10^{-7}	-4.88682×10^{-7}

2.2 Pressure effect

Oxygen has a pressure effect due to the stability of the luminophore's excited state L* itself, the O2 activity inside the sensing foil, and the pressure response of luminescence quenching [Bittig et al., 2018].

The pressure compensation factor is calculated as:

$$p_{\text{factor}} = \left(\frac{|P|}{100}\right) \cdot C_p + 1$$

where

- P is the pressure from the CTD (dbar),
- C_p is the pressure correction calibration coefficient provided on the sensor calibration certificate.

2.3 Impact on data

The salinity and pressure correction increased oxygen concentrations measured by the Aanderaa sensors by approximately 1.5–33%, with a standard deviation of 9%, relative to the uncorrected values (Figure 2). In contrast, oxygen concentrations collected by the Rinko sensor decreased by approximately 17–20%, with a standard deviation of 0.4%, following correction (Figure 3).

The internal reference salinity is the salinity value assumed by the optode software when applying the salinity correction. C-PROOF Aanderaa sensors were specially programmed with an internal reference salinity of 35 PSU, based on typical conditions in the Northeast Pacific, rather than the default value of 0 PSU to reduce known this bias. The larger salinity bias observed for the Rinko optodes is explained by their assumed internal reference salinity of 0 PSU (Figure 3b). The salinity correction factor (s_{factor}) has a mean and standard deviation of 0.806 and 0.007, respectively, for the Rinko optodes, compared with 1.008 and 0.004 for the Aanderaa optodes (Figure 2b). Conversely, the pressure correction factor (p_{factor}) is larger for the Aanderaa optodes, with a mean and standard deviation of 1.2 and 0.1 (Figure 2c), compared with 1.005 and 0.005 for the Rinko optodes (Figure 3c).

Using the adjusted CTD data instead of the raw CTD data has a negligible effect on the pressure and salinity correction applied to the oxygen measurements. A salinity error of 0.2 PSU changes the pressure- and salinity-corrected oxygen concentration by an average of 0.13% (approximately 0.11 μmol L^{-1}) and by up to 0.14% (approximately 0.42 μmol L^{-1}) across the dataset. We nevertheless use the adjusted CTD data because it represents the most accurate salinity measurements after correcting for thermal lag.

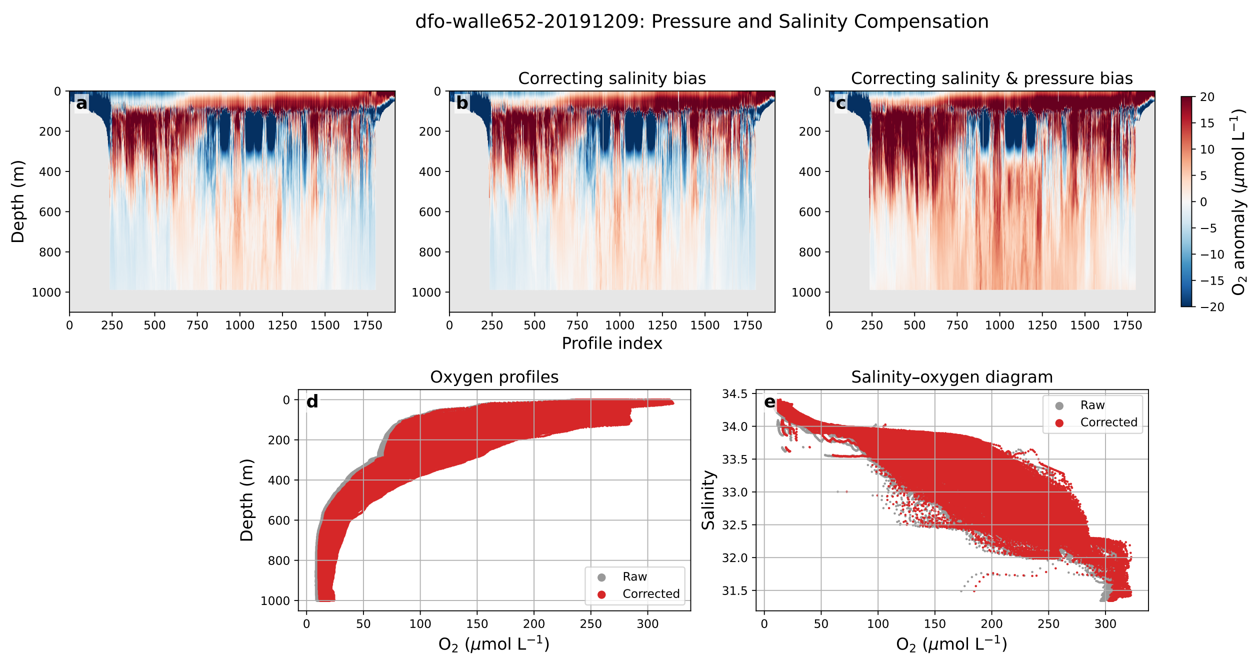

Figure 2: dfo-walle652-20191209 with Aanderaa optode 4381: Oxygen anomalies from mean raw[O_2] at each depth using a) raw O_2 b) [O_2] corrected for the salinity bias (c) corrected for salinity and pressure biases ([O_2,PS]) d) [O_2,PS] (red) and Raw O_2 (gray) profiles with depth e) [O_2,PS] on levels of constant salinity.

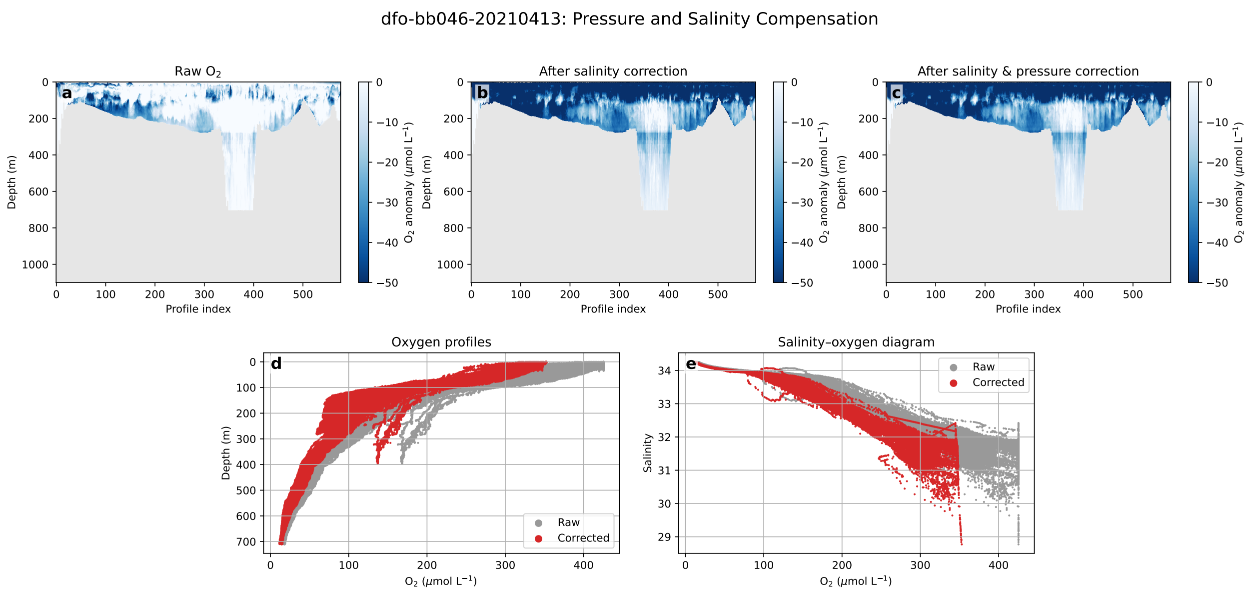

Figure 3: dfo-bb046-20210413 with Rinko AROD-FD otpode: Oxygen anomalies from mean raw[O_2] at each depth using a) raw O_2 b) [O_2] corrected for the salinity bias c) corrected for salinity and pressure biases ([O_2,PS]). d)[O_2,PS] (red) and Raw O_2 (gray) profiles with depth e) [O_2,PS] on levels of constant salinity.

3 Flag Spikes and Bad Data

We flag good data as QC 1 and bad data as QC 4, following Argo quality-control notation (see `https://argo.ucsd.edu/data/how-to-use-argo-files/`). Oxygen optodes are not pumped like the Glider Pumped CTD (GPCTD) used on some gliders, where biological material can build up in the tubing, especially in highly productive regions (see the C-PROOF GPCTD processing report). Although less common, material can stick to an optode and produce bad oxygen data. For mission dfo-bb046-20210413, data after profile 579 are flagged as QC 4 (Figure 4).

A more robust flagging method should be developed to identify small-scale spikes that are not removed by the time-response correction or by gridding, where data are averaged into one-metre depth bins.

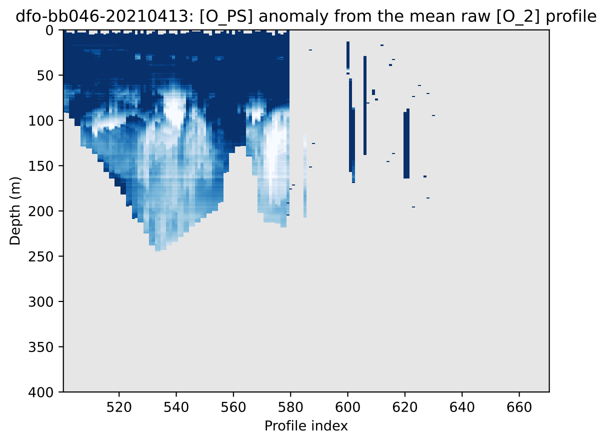

Figure 4: Oxygen anomalies for dfo-bb046-20210413 with a Rinko AROD-FD optode. Anomalies are calculated relative to the mean raw $[O_2]$ at each depth using $[O_2]$ corrected for salinity and pressure biases.

4 Convert [O_2] from μmol/L to μmol/kg

We convert [O_2,PS] to μmol/kg, the more commonly used units. The following corrections are all computed in μmol/kg.

5 Sensor response time lag correction

This finite response time of the optode causes the measured oxygen concentration to lag behind rapid environmental changes, attenuating sharp oxygen gradients. Because the sensor requires time to equilibrate with the surrounding water, oxygen transitions are recorded after the glider has already moved past them. During downcasts this shifts features deeper, whereas during upcasts the same lag shifts them shallower, producing systematic upcast/downcast asymmetry (e.g., Figure 1a). The response time depends on temperature and stagnant boundary layer thickness. Bittig et al. [2014] suggests that τ is expected to fall between 25 - 80 s for Aanderaa sensors on gliders in the temperature range experienced in the Northeast Pacific (Figure 5) and 1-3 s for Rinko sensors when being sampled by a glider. We apply the sharpening filter using a mission-specific response time, τ, to the pressure- and salinity-compensated oxygen concentration to account for the difference in environment and flow speed.

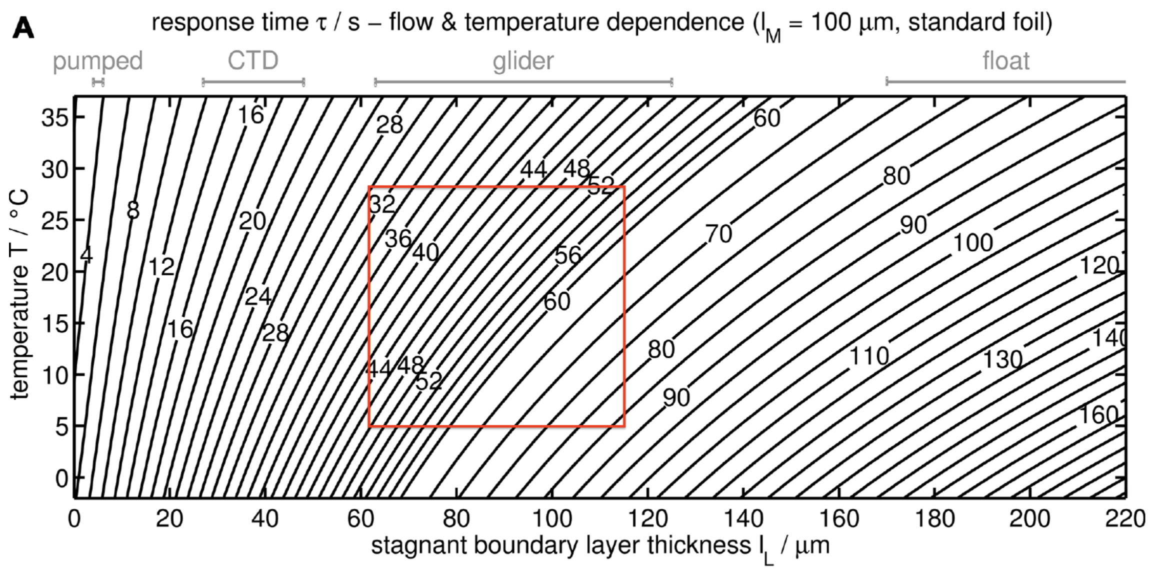

Figure 5: Experimentally estimated response times for Aanderaa 3820 and 4330 optodes influenced by temperature, mixed layer thickness and speed. The red box includes expected response times based on conditions observed by gliders in the Northeast Pacific. Modified Figure 11A from Bittig et al. [2014].

[Bittig et al., 2014] made an equation is a model to reverse the effect of the time-response on oxygen data:

$$[O_{2,PS}]_{\text{measured},\, i} = a[O_{2,PS}]_{\text{measured},\, i-1} + b[O_{2,PS}]_{\text{true},\, i} \tag{3}$$

with

- $a = \exp\left(-\frac{\Delta t_i}{\tau}\right)$,
- $b = 1 - a$

where $\Delta t_i = t_i - t_{i-1}$.

To compensate for this lag, a *sharpening filter*, i.e. the inverse of Equation 4, is applied to [O_2,PS]:

$$[O_{2,PS}]_{\text{true},\, i} = \frac{[O_{2,PS}]_{\text{measured},\, i+1} - a[O_{2,PS}]_{\text{measured},\, i}}{2b}, \tag{4}$$

with

- $b = \frac{1}{1+2\tau/\Delta t_i}$
- $a = 1 - 2b$.

The sharpening filter shifts oxygen transitions in upcasts downward and downcast transitions upward (Figure 10; Figure 1c), bringing regions of large oxygen gradients into closer depth alignment. It also reduces the phase shift introduced by the sensor response, decreasing the area enclosed between adjacent upcasts and downcasts in oxygen-depth space since the equation has a phase component.

5.1 Time response: Aanderaa

The response time, (τ), must be estimated separately for each glider mission because it depends on environmental conditions such as temperature and flow speed. Following the approach described above, a range of candidate response times (25–80 s) was evaluated by applying the sharpening filter and quantifying the agreement between adjacent upcasts and downcasts.

A mission-specific response time, τ, is estimated by minimizing the following objective function, calculated from 20 consecutive oxygen profiles between the average depth of the oxycline (approximately 70–150 m) and 1000 m after applying the sharpening filter (Equation 4):

$$\frac{(\Delta O_2)^2}{\sigma(O_{2,\mathrm{iso}})}\frac{N_0}{N} \tag{5}$$

where N_0 is the number of finite oxygen profiles and N is the total number of profiles (e.g,. Figure 6). The optimization produces a broad, bowl-shaped minimum spanning approximately 20 s, indicating that a range of response times produces similarly small profile differences.

The oxycline is identified as the sharp transition in $[O_{2,\mathrm{PS}}]$ (e.g., Figures 2 and 3a–c). The upper ocean was excluded because it exhibits strong natural oxygen gradients associated with the oxycline, and relatively few paired upcast/downcast observations are available near the surface. Including this region would therefore disproportionately influence the optimization. The objective function was weighted by the number of observations contributing at each depth, reducing the influence of sparsely sampled deep waters while emphasizing well-sampled regions of the profile.

For mission dfo-walle652-20191209, a response time of 55 s was selected because it minimizes the objective function below the oxycline (Figure 7 b). Response times within approximately ± 10 s produce similar reductions in upcast/downcast asymmetry (Figure 7a,b,c; 8a,b,c), indicating that the optimization is relatively insensitive within this range. The dfo-walle652-20191209 mission experienced a range of flow speeds and temperatures that influence the sensor response time. Averaging over these varying environmental conditions likely broadens the minimum in the objective function (Figure 5).

Although alternative optimization strategies may further reduce errors near the oxycline, we concluded that estimating a single mission-specific response time provides a simple, computationally efficient correction that performs well below the mixed layer. Because the optimal response time varies among sensors and deployments (e.g. Figure 9), τ should be estimated independently for each mission.

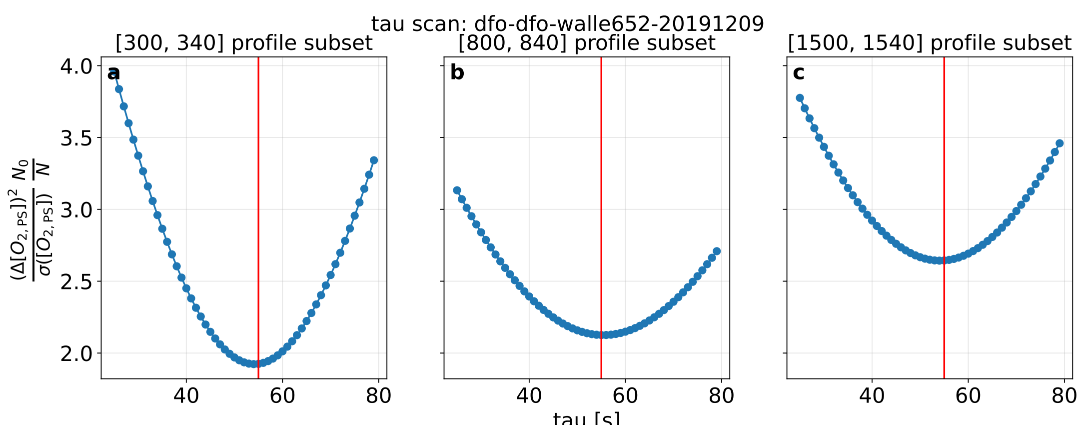

Figure 6: Example using dfo-walle652-20191209 with an Aanderaa O2 optode: Objective function used to estimate the mission-specific response time for three groups of consecutive profiles (a)300-340, (b) 800-840, (c)1400-1440 below 150 m. The optimum response time selected for this mission is 55 s (red).

The sharpening filter does not work well at small time scales and amplifies high-frequency variability because it is the inverse of the optode's low-pass sensor response [Bittig et al., 2014]. The observed oxygen spectrum is approximately consistent with red-noise behaviour, with most variance occurring at low frequencies (Figure 13yellow,brown). Consequently, applying the sharpening filter preferentially amplifies

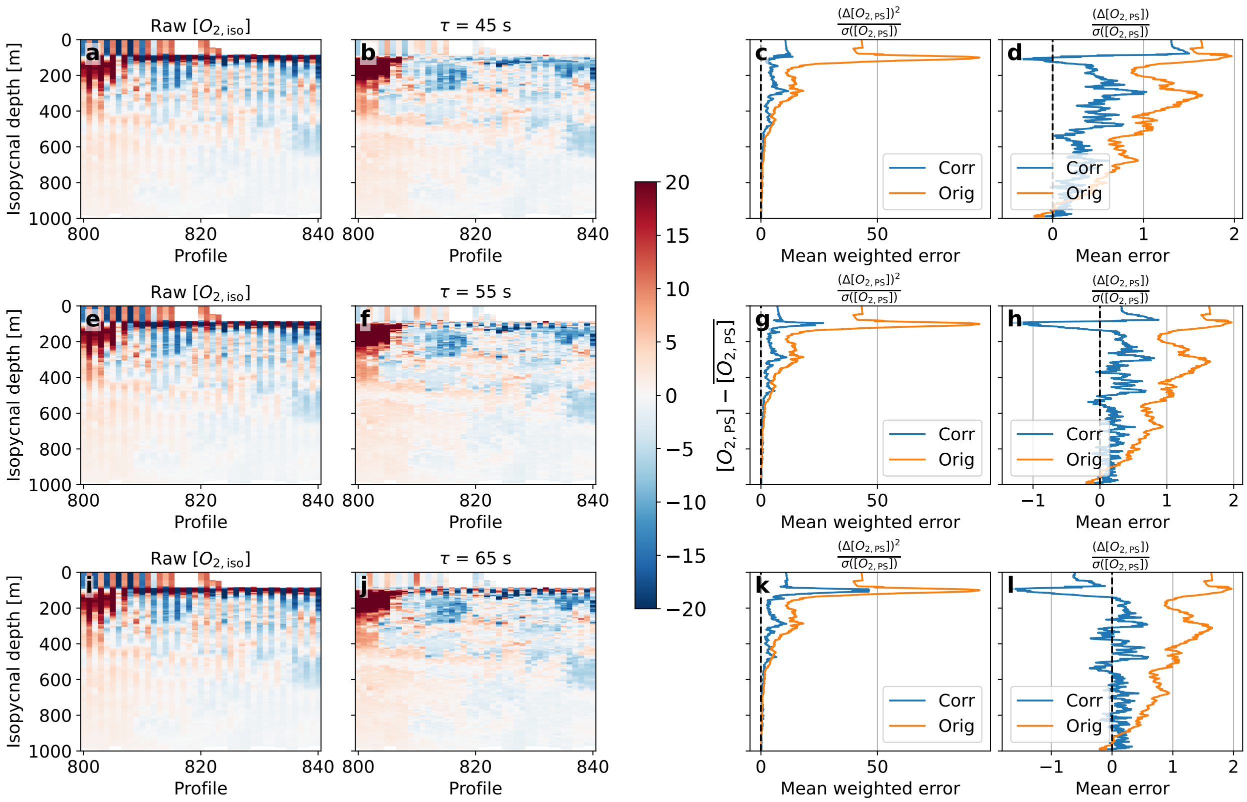

Figure 7: Example using mission dfo-walle652-20191209 with an Aanderaa optode. (a,e,i) Oxygen anomaly in isopycnal space, calculated as $[O_{2,\mathrm{PS}}] - \overline{[O_{2,\mathrm{PS}}]}$, using the raw oxygen measurements. (b,f,j) Oxygen anomaly after applying the sharpening filter with response times of 55, 45, and 65 s, respectively. (c,g,k) Mean depth-dependent weighted objective function, $\frac{(\Delta[O_{2,\mathrm{PS}}])^2}{\sigma([O_{2,\mathrm{PS}}])}\frac{N_0}{N}$, calculated from the raw (blue) and corrected (orange) oxygen measurements. (d,h,l) Mean depth-dependent normalized squared oxygen difference, $\frac{(\Delta[O_{2,\mathrm{PS}}])^2}{\sigma([O_{2,\mathrm{PS}}])}$, calculated from the raw (blue) and corrected (orange) oxygen measurements. All panels show profiles 800–840.

high-frequency noise, which is evident in both the oxygen time series (10) and the corresponding power spectra (Figure12).

To limit the amplification of isolated spikes, we first smooths the pressure- and salinity-corrected oxygen record with a 1.5 s (three-sample) running mean before applying the sharpening filter. After the sharpening filter is applied, the corrected oxygen record is smoothed using a window of approximately $(\tau/2)$ s. This second smoothing step suppresses the high-frequency variability introduced by the inverse filter while preserving the low-frequency oxygen variability (Figures11, 13 red).

A more sophisticated method may improve corrections in the upper ocean, where the sharp oxycline remains difficult to align. For example, even after time-response correction, the downcast oxycline is typically observed approximately 3 m shallower than the upcast oxycline (e.g., Figure 10a,d; Figure 1b). We experimented with alternative methods to estimate τ, but concluded that they provided negligible improvement while substantially increasing computational complexity or introducing additional error.

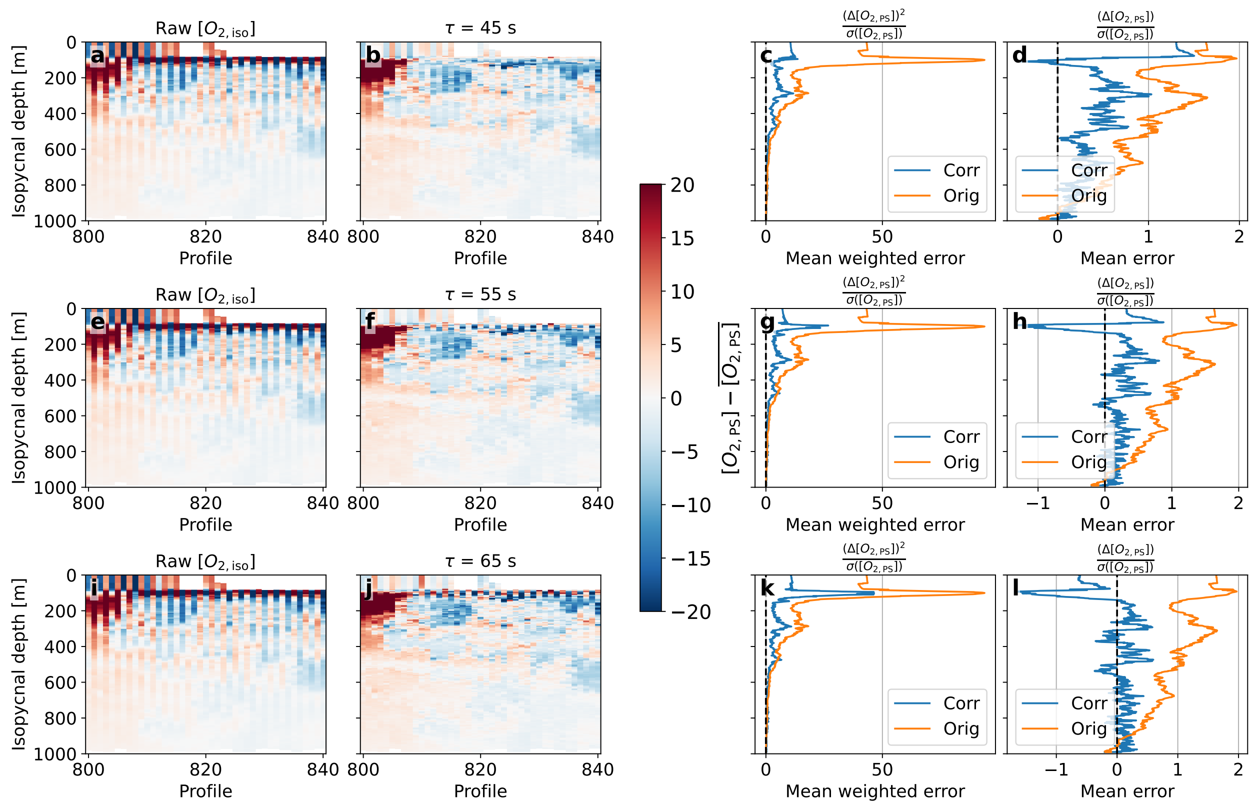

Figure 8: Example using mission dfo-walle652-20191209 with an Aanderaa optode. (a,e,i) Oxygen anomaly in isopycnal space, calculated as $[O_{2,\mathrm{PS}}] - \overline{[O_{2,\mathrm{PS}}]}$, using the raw oxygen measurements. (b,f,j) Oxygen anomaly after applying the sharpening filter with response times of 55, 45, and 65 s, respectively. (c,g,k) Mean depth-dependent weighted objective function, $\frac{(\Delta[O_{2,\mathrm{PS}}])^2}{\sigma([O_{2,\mathrm{PS}}])}\frac{N_0}{N}$, calculated from the raw (blue) and corrected (orange) oxygen measurements. (d,h,l) Mean depth-dependent normalized squared oxygen difference, $\frac{(\Delta[O_{2,\mathrm{PS}}])^2}{\sigma([O_{2,\mathrm{PS}}])}$, calculated from the raw (blue) and corrected (orange) oxygen measurements. All panels show profiles 1500–1540.

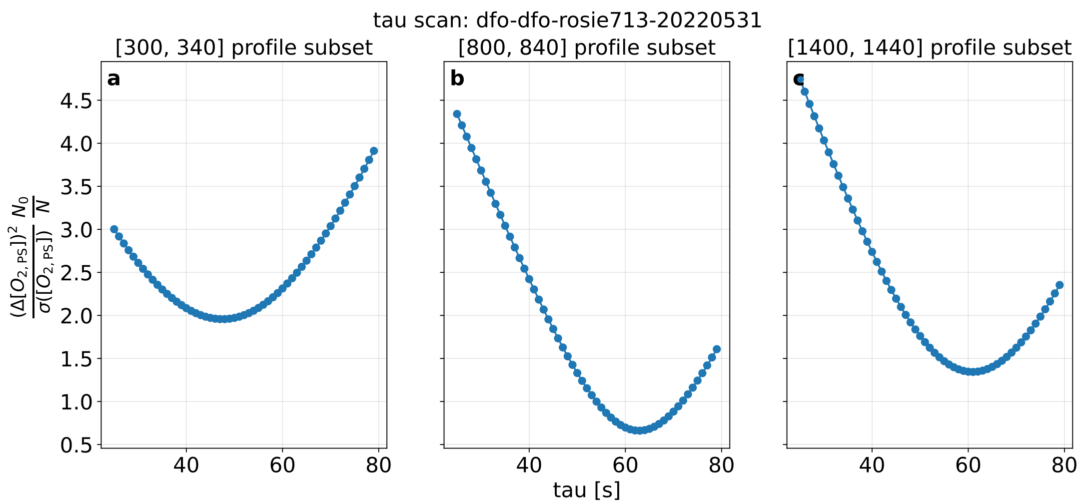

Figure 9: Example using mission dfo-rosie713-20220531 with an Aanderaa optode. Objective function used to estimate the mission-specific response time for three groups of consecutive profiles: (a) 300–340, (b) 800–840, and (c) 1400–1440. The objective function is calculated as $\frac{(\Delta[O_{2,\mathrm{PS}}])^2}{\sigma([O_{2,\mathrm{PS}}])}\frac{N_0}{N}$ after applying the sharpening filter using a range of candidate response times. The optimum response time selected for this mission is 55 s (red).

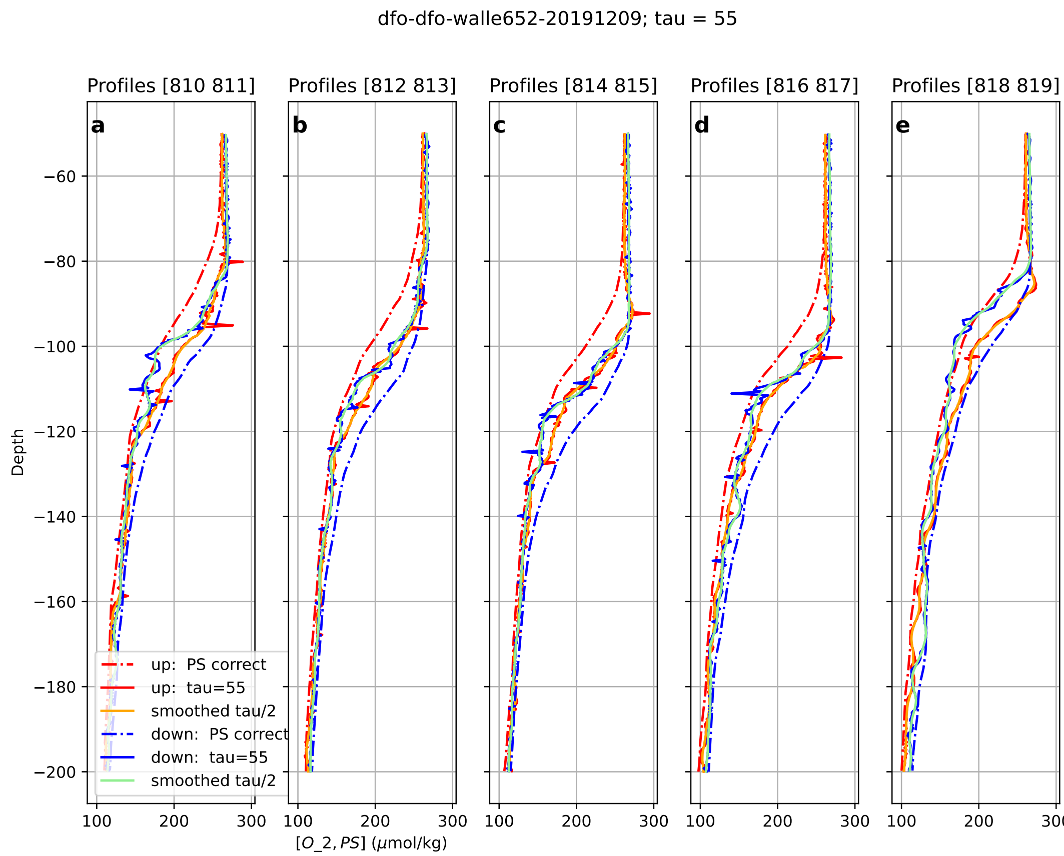

Figure 10: Example using mission dfo-walle652-20191209 with an Aanderaa optode. Pressure- and salinity-corrected oxygen before ([$O_{2,PS}$; dashed) and after ([O_τ, solid) time-response correction using a sharpening filter with $\tau = 55$ s. Adjacent downcasts (blue) and upcasts (red) are shown for five representative profile pairs.

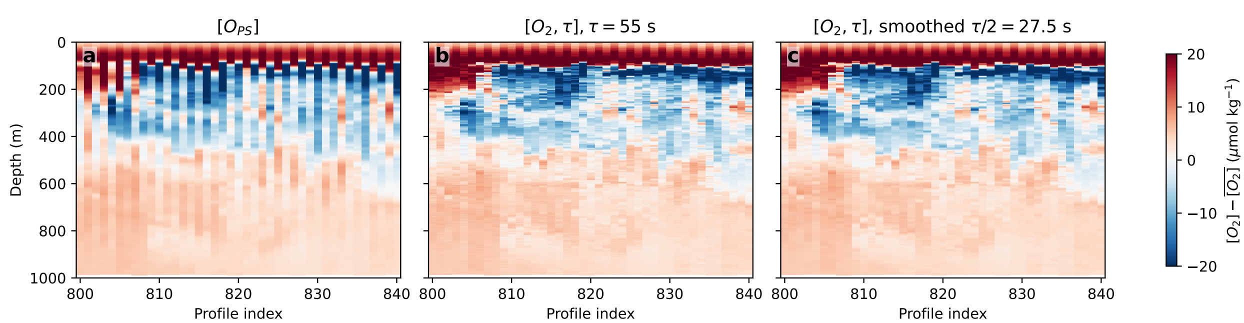

Figure 11: Example using mission dfo-walle652-20191209 with an Aanderaa optode. (a) Raw oxygen measurements, [$O_{2,PS}$] (b) Pressure- and salinity-corrected oxygen after applying the sharpening filter with $\tau = 55$ s, [O_τ]. (c) [O_τ] after subsequent smoothing with a running mean of $\tau/2$ (27.5 s).

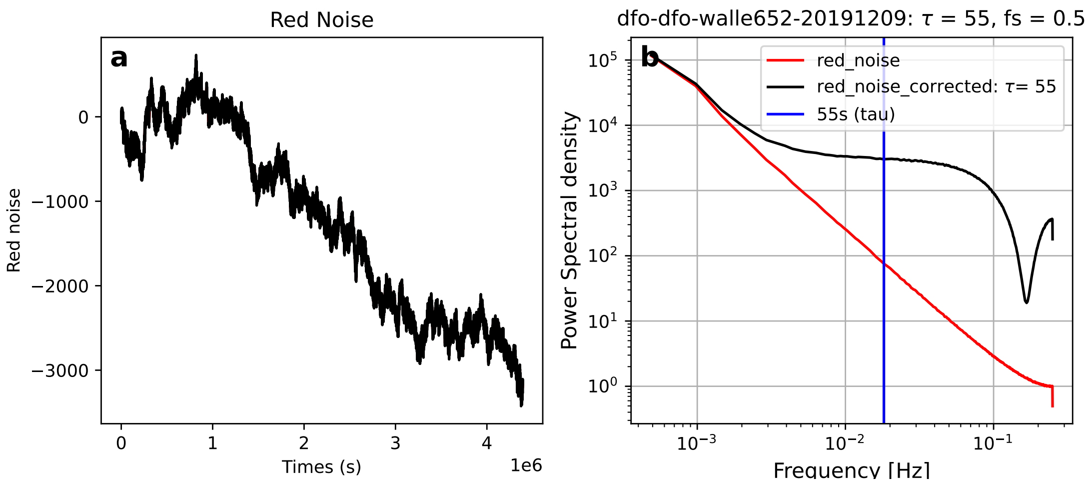

Figure 12: (a) Randomly generated red noise the length of the dfo-walle652-20191209 oxygen timeseries. (b) Spectrum of the red noise timeseries (red) and red noise timeseries passed through the sharpening filter with τ= 55 s (black) from (equation 4, Bittig et al. [2014]) calculated using the Welch method with segment lengths of 1024. The scale of τ= 55 s is marked in blue.

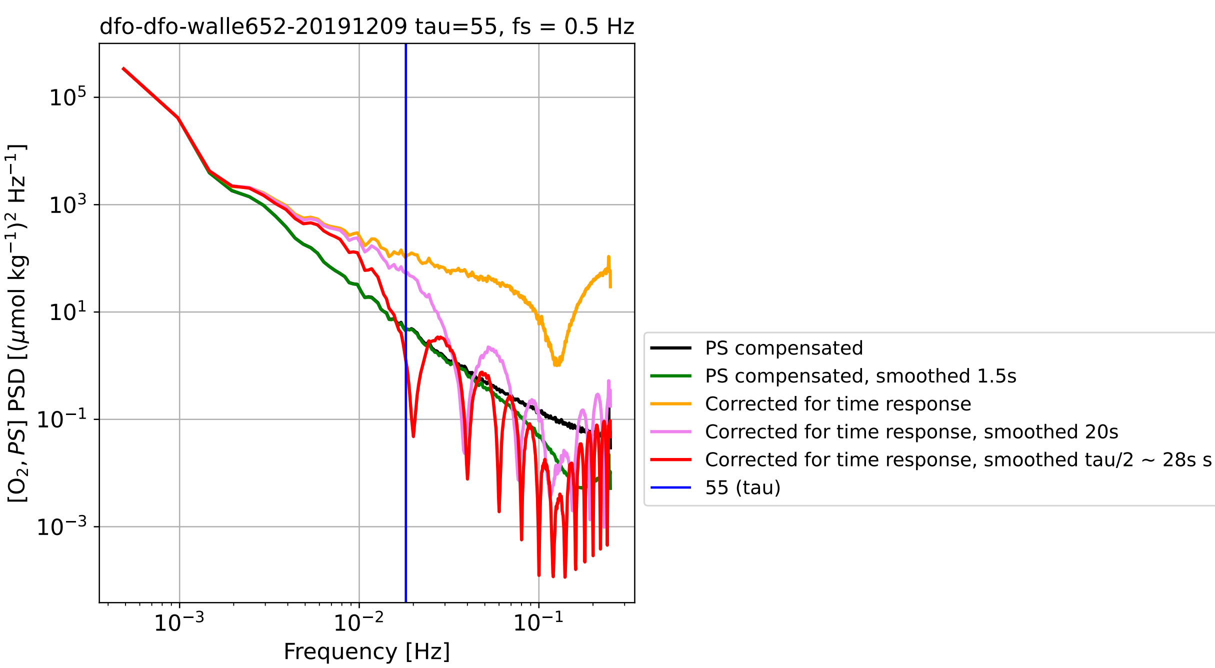

Figure 13: Power spectral density of oxygen for mission dfo-walle652-20191209 with an Aanderaa optode. Spectra are shown for pressure- and salinity-corrected oxygen $[O_{2,PS}]$ (black), $[O_{2,PS}]$ after 1.5 s pre-smoothing (green), after pre-smoothing and time-response correction with $\tau = 55$ s ($[O_\tau]$, orange), and after the subsequent post-filter smoothing using a running mean of $\tau/2$ (27.5 s; red). The vertical blue line marks the characteristic frequency corresponding to $\tau = 55$ s.

5.2 Other approaches to time response correction

There is no agreed-upon method for finding τ to substitute into Bittig et al. [2014]'s sharpening filter (Equation 4) in the glider community (See `https://oceangliderscommunity.github.io/Oxygen_SOP/sections/oxygen_introduction.html`), which lead us to experimenting with different methods. We will introduce the approaches we tried and explain their limitations.

5.2.1 Alternative methods of finding tau in μmol/kg

We attempted finding a method to determine τ(s) to substitute into Equation 4 that aligns the up and downcasts better in space, especially near the oxycline (e.g., Figure 10a,d; Figure 1b).

Test a) Independently optimize τ in the upper and lower layers

We attempted using a finding an upper-layer and lower-layer response time using the same optimization procedure described for the single-(τ) case, except that the objective function was evaluated only above the oxycline (Figure 14d,e,f). For dfo-walle652-20191209, the optimization was restricted to depths shallower than 75 m to avoid including variability associated with the oxycline (Figure 14a,b,c). The time response was taken to be 25 s, but it did not converge that that τ, suggesting the optimal τ is out of the range expected based on the physics of this optode in the conditions experienced by the C-PROOF fleet (Figure 5), suggesting this is not the best method.

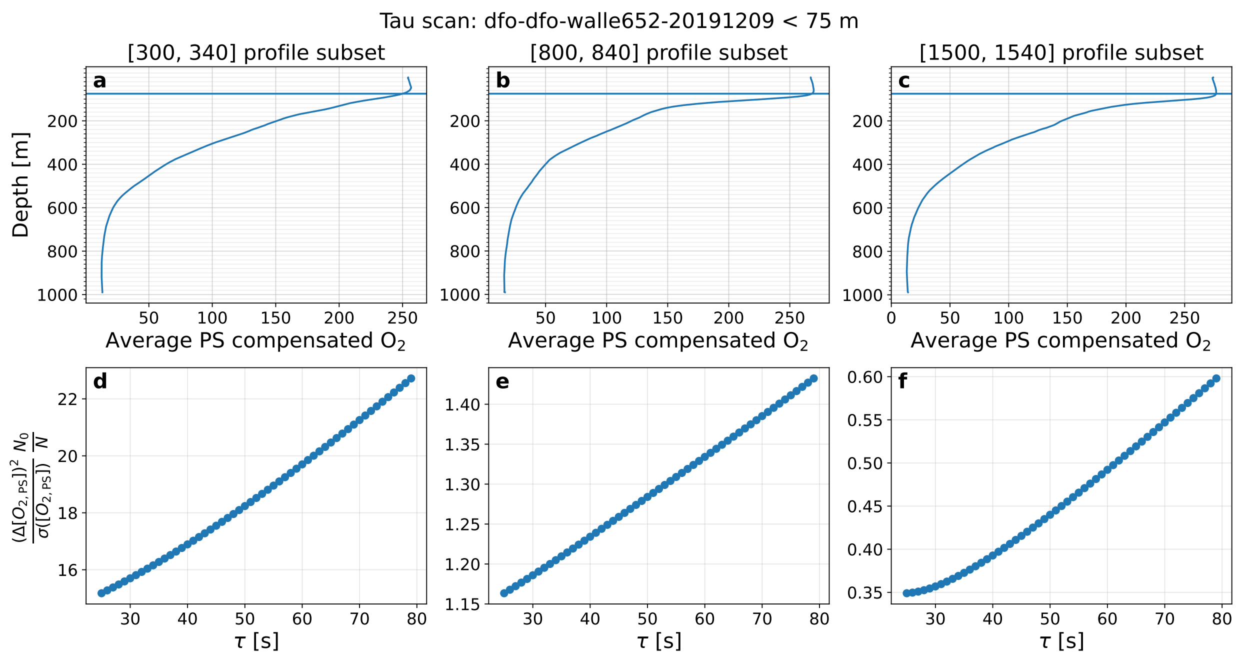

Figure 14: Example using dfo-walle652-20191209 with an Aanderaa O2 optode: Mean pressure-salinity (PS) compensated oxygen profiles for profile groups: (a) 300-340, (b) 800-840, (c) 1500-1540. Objective function used to estimate the mission-specific response time for three groups of consecutive profiles (d) 300-340, (e) 800-840, (f) 1400-1440.

Applying $\tau = 25$ s above 75 m and $\tau = 55$ s below 75 m reduces the upcast/downcast asymmetry relative to the pressure- and salinity-corrected oxygen measurements (Figure 15d). However, substantial variability remains within the upper water column, similar to that observed when a single mission-specific response time is applied (Figure 15b,c).

The upper–lower layer boundary was chosen to lie above the oxycline (75 m). Including the oxycline in the upper-layer optimization by moving the boundary to approximately 100 m results in poorer agreement between adjacent upcasts and downcasts (Figure 16).

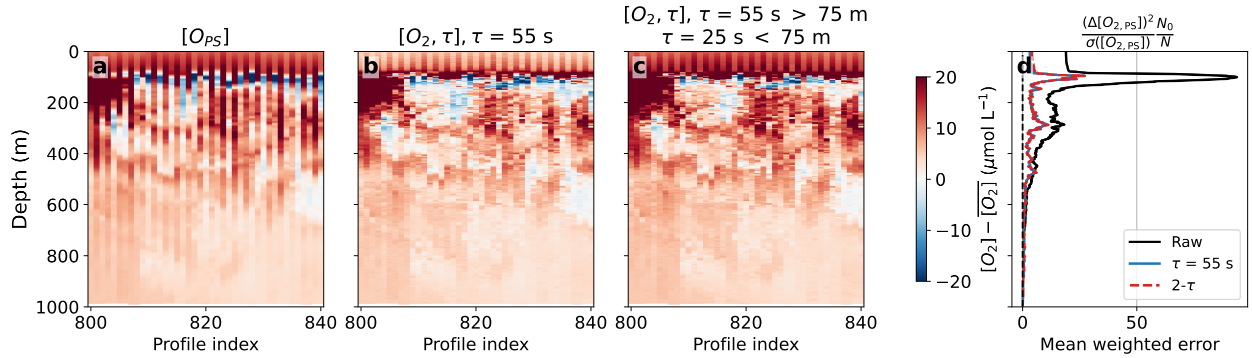

Figure 15: Example using mission dfo-walle652-20191209 (profiles 800–840) with an Aanderaa optode. (a) Oxygen anomaly in depth space, calculated as $[O_{2,\text{PS}}] - \overline{[O_{2,\text{PS}}]}$, using the raw oxygen measurements. (b) Oxygen anomaly after time-response correction using a sharpening filter with $\tau = 55$ s. (c) Oxygen anomaly after applying a two-τ correction, with $\tau = 55$ s below 75 m and $\tau = 25$ s above 75 m. (d) Mean depth-dependent weighted objective function, $\frac{(\Delta[O_{2,\text{PS}}])^2}{\sigma([O_{2,\text{PS}}])}\frac{N_0}{N}$, calculated from the raw (black), single-τ (blue), and two-τ (red) oxygen measurements.

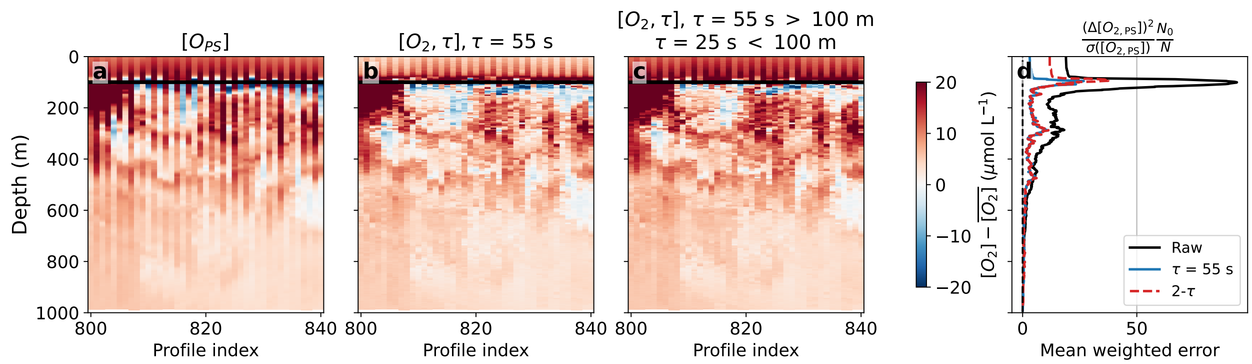

Figure 16: Example using mission dfo-walle652-20191209 (profiles 800–840) with an Aanderaa optode. (a) Oxygen anomaly in depth space, calculated as $[O_{2,\text{PS}}] - \overline{[O_{2,\text{PS}}]}$, using the raw oxygen measurements. (b) Oxygen anomaly after time-response correction using a sharpening filter with $\tau = 55$ s. (c) Oxygen anomaly after applying a two-τ correction, with $\tau = 55$ s below 100 m and $\tau = 25$ s above 100 m. (d) Mean depth-dependent weighted objective function, $\frac{(\Delta[O_{2,\text{PS}}])^2}{\sigma([O_{2,\text{PS}}])}\frac{N_0}{N}$, calculated from the raw (black), single-τ (blue), and two-τ (red) oxygen measurements.

Overall, the two-τ approach provides no significant improvement over a single mission-specific response time. Given the additional computational complexity and the lack of a well-constrained upper-layer optimum, we concluded that the improvement does not justify adopting this approach.

Test b) Optimize tau in lower layer, then scale the upper layer τ based on Bittig et al. [2014] Bittig et al. [2014] showed that optode response time depends on both glider speed and temperature. Because C-PROOF gliders generally maintain a constant speed throughout each mission, with only modest variations due to ocean currents and turning near the surface (Figure 17), we investigated whether the upper-layer response time could be estimated by scaling the optimized lower-layer response time rather than fitting it independently.

The upper-layer response time was estimated from the lower-layer response time using:

$$\tau = \tau_{\text{low}} \frac{v_{\text{up}}}{v_{\text{low}}} * \text{temperature scaling} \tag{6}$$

where τ_{low} is the optimized response time below the oxycline, v_{low} is the mean glider speed below the oxycline, and v_{up} is the mean glider speed above the oxycline. Two temperature-scaling approaches were evaluated: (a) a constant scaling factor of 0.8, assuming that warmer near-surface temperatures reduce τ by approximately 20% Bittig et al. [2014]; and

(b) an exponential scaling referenced to the mean temperature below the oxycline:

$$\text{temperature scaling} = k^{0.05(T - T_{ref})} \tag{7}$$

.

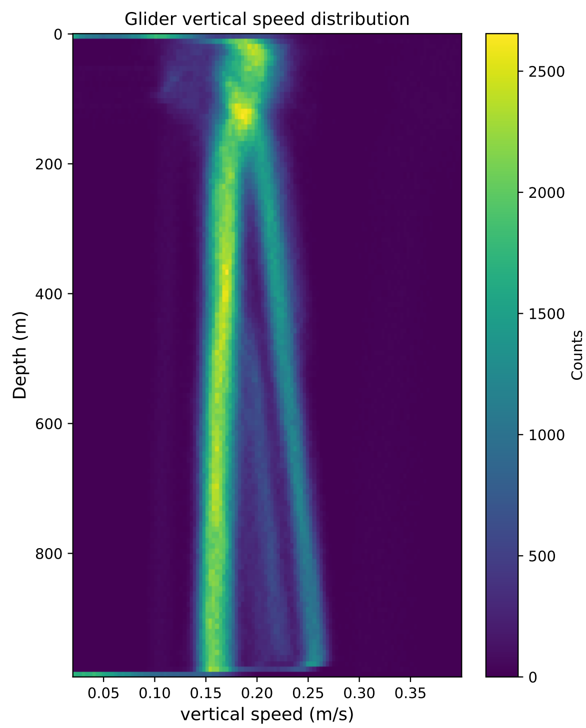

Figure 17: 2D histogram of vertical speed with depth of mission dfo-walle652-20191209.

For most C-PROOF missions, the glider slows in the upper approx. 20 m while changing direction (e.g., Figure 18). Using only the speed scaling (approach a) reduced the upper-layer response time to approximately 35 s, which remained 10 s larger than the independently optimized value of 25 s (which we discussed did not converge, suggesting this method is not reliable).

For dfo-walle652-20191209, speed scaling alone produced little change in τ from what we used in option a (fitting τ to the upper layer, though it did not converge). In contrast, the exponential temperature scaling

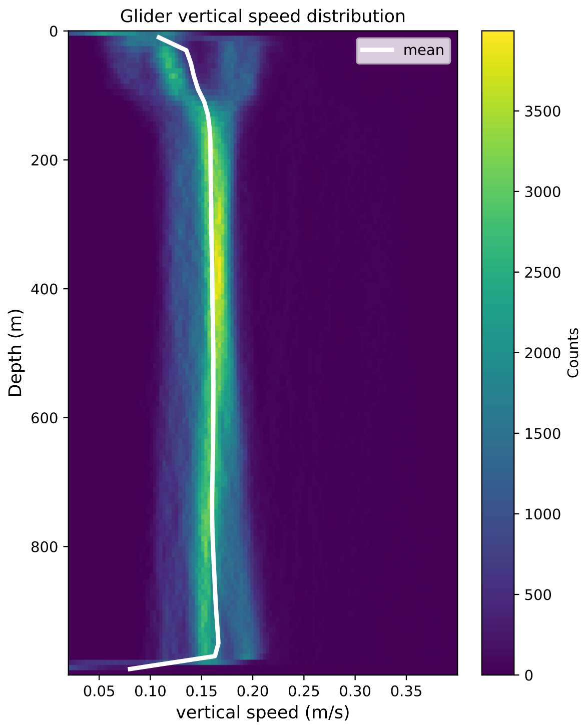

Figure 18: 2D histogram of vertical speed with depth of mission dfo-rosie713-20230810. The mean speed at every depth is plotted in white.

(approach b), referenced to a lower-layer temperature of 4.6C, produced an upper-layer response time of approximately 25 s for both dfo-walle652-20191209 and dfo-rosie713-20230810.

Although the scaling approaches occasionally reduced the disagreement between adjacent upper-water-column profiles, neither consistently outperformed the single mission-specific τ approach (Figure 19).

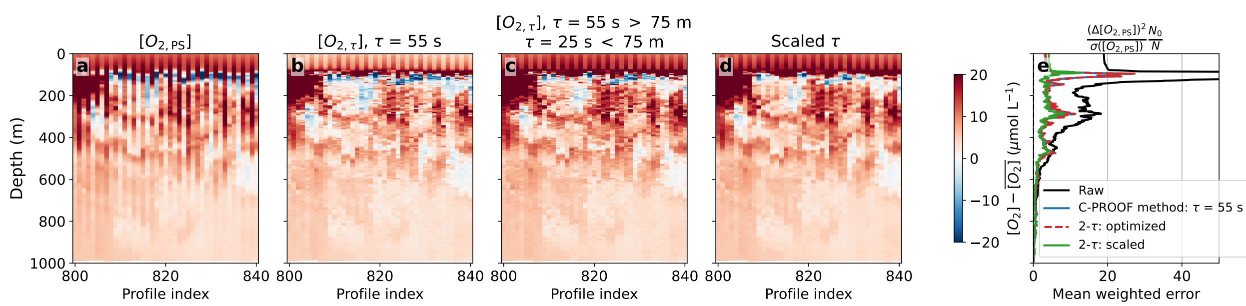

Figure 19: (a) Example using dfo-walle652-20191209 profiles 1100-1140 with Aanderaa O2 optode: τ scaled by temperature and vertical speed following [Bittig et al., 2014]. Lower τ is expected at higher temperatures and slower speeds near the surface. (b) $[O_2]$ after applying sharpening filter with τ=55s. (c) $[O_2]$ after applying sharpening filter with time-specific τ from (a). (c) Mean squared difference between [O_2] profiles normalized by the standard deviation of oxygen along isopyncals for raw oxygen data (black), corrected with τ=55 s for the entire water column (blue) and corrected with time-varying τ (orange).

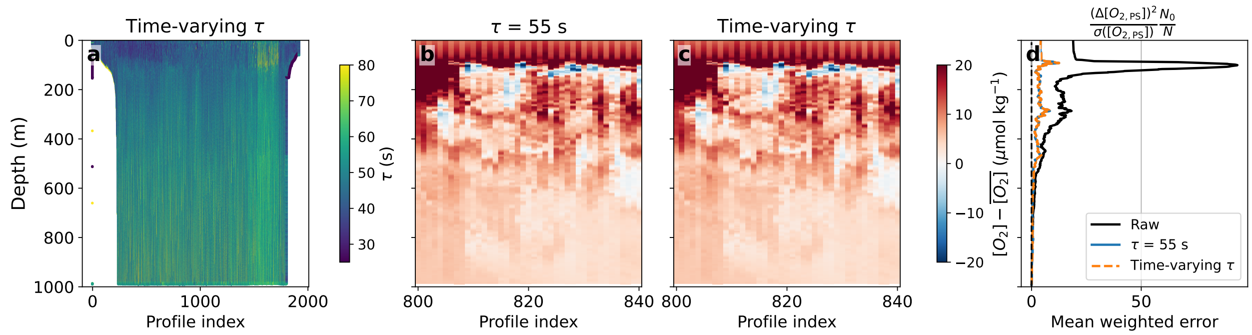

Figure 20: Example using mission dfo-walle652-20191209 with an Aanderaa optode. (a) Time-varying response time, τ, calculated from the local temperature and glider speed using a reference response time of 55 s at 5°C and a glider speed of 0.17 m s^{-1}. (b) Oxygen anomaly in depth space, calculated as $[O_{2,\mathrm{PS}}] - \overline{[O_{2,\mathrm{PS}}]}$, after applying a single mission-specific response time of $\tau = 55$ s for profiles 800-840. (c) Oxygen anomaly after applying the time-varying response time shown in (a) for profiles 800–840. (d) Mean depth-dependent weighted objective function, $\frac{(\Delta[O_{2,\mathrm{PS}}])^2}{\sigma([O_{2,\mathrm{PS}}])}\frac{N_0}{N}$, calculated from the raw (black), single-τ (blue), and time-varying τ (green) oxygen measurements.

Option C: Time varying τ

We also evaluated a time-varying τ, scaling each glider measurement according to its temperature and speed relative to a reference value of $\tau = 55$ s at 5°C and a glider speed of 0.17 m s^{-1}. The resulting correction was not sufficiently different from the single-τ approach to justify the additional computational cost (Figure 20.

5.2.2 Alternative approaches of finding tau

There are additional approaches to how to find τ suggested by the greater glider community (See `https://oceangliderscommunity.github.io/Oxygen_SOP/sections/oxygen_introduction.html`), however we stuck to a single-optimized τ for its simplicity and improvement.

One method suggested, which was implemented on some publications using C-PROOF data (ex. Stevens et al., Hare et al., Ross et al.), estimates τ using the least squares equation from Fofonoff et al. [1974]:

$$phase_{true} = phase_{measured} + \tau \cdot d/dt \cdot phase_{measured} \tag{8}$$

Here, $\mathrm{phase}_{\mathrm{measured}}$ is the calibrated optode phase, $\mathrm{phase}_{\mathrm{true}}$ is the estimated true phase, and d/dt denotes the first derivative with respect to time along an individual upcast or downcast.

This approach requires converting dissolved oxygen concentration back to optode phase before estimating τ. Because this additional conversion may introduce further uncertainty, C-PROOF instead adopted an approach that estimates τ directly from oxygen concentration by minimizing the difference between adjacent upcast and downcast profiles after applying the sharpening filter. This optimization strategy is analogous to the approach used to determine the thermal-lag correction constants for the Glider Payload CTD (see the C-PROOF GPCTD Processing Report for details).

5.3 Time response: Rinko

Rinko optodes have a fast response time of approximately 0–4 s [Bittig et al., 2014], requiring little or no time-response correction. As with the Aanderaa processing, a mission-specific response time was estimated by minimizing the objective function described above. For many C-PROOF missions, including dfo-bb046-20210413, the optimum response time was effectively zero (Figures 21 and 22), indicating that no measurable lag correction is required. Consistent with this result, the raw Rinko observations do not exhibit the pronounced upcast/downcast asymmetry characteristic of the Aanderaa optodes (Figure 11a).

Because no sharpening filter is applied when the optimum response time is zero, the pressure- and salinity-corrected oxygen ([O_{PS}]) is not pre-smoothed. Likewise, no post-filter smoothing is applied. For missions with a small but non-zero optimum response time (e.g., $\tau < 3$ s), post-filter smoothing is also omitted because it produces negligible changes in the corrected oxygen concentrations while unnecessarily reducing temporal resolution.

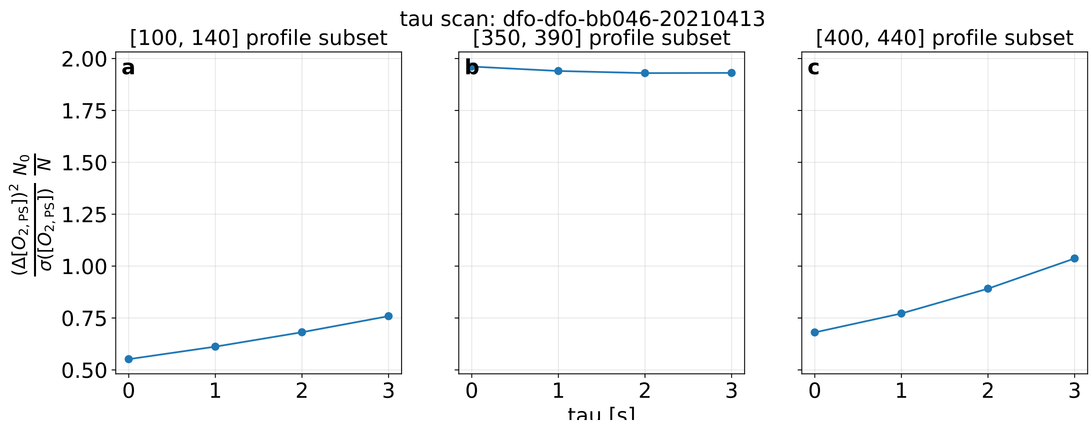

Figure 21: Example using dfo-bb046-20210413 with an Rinko O2 optode: Objective function used to estimate the mission-specific response time for three groups of consecutive profiles (a)100-140, (b) 300-340, (c)400-440. below 150m The time response, τ, used for this mission is 0s, following the expected range for the optode [Bittig et al., 2014].

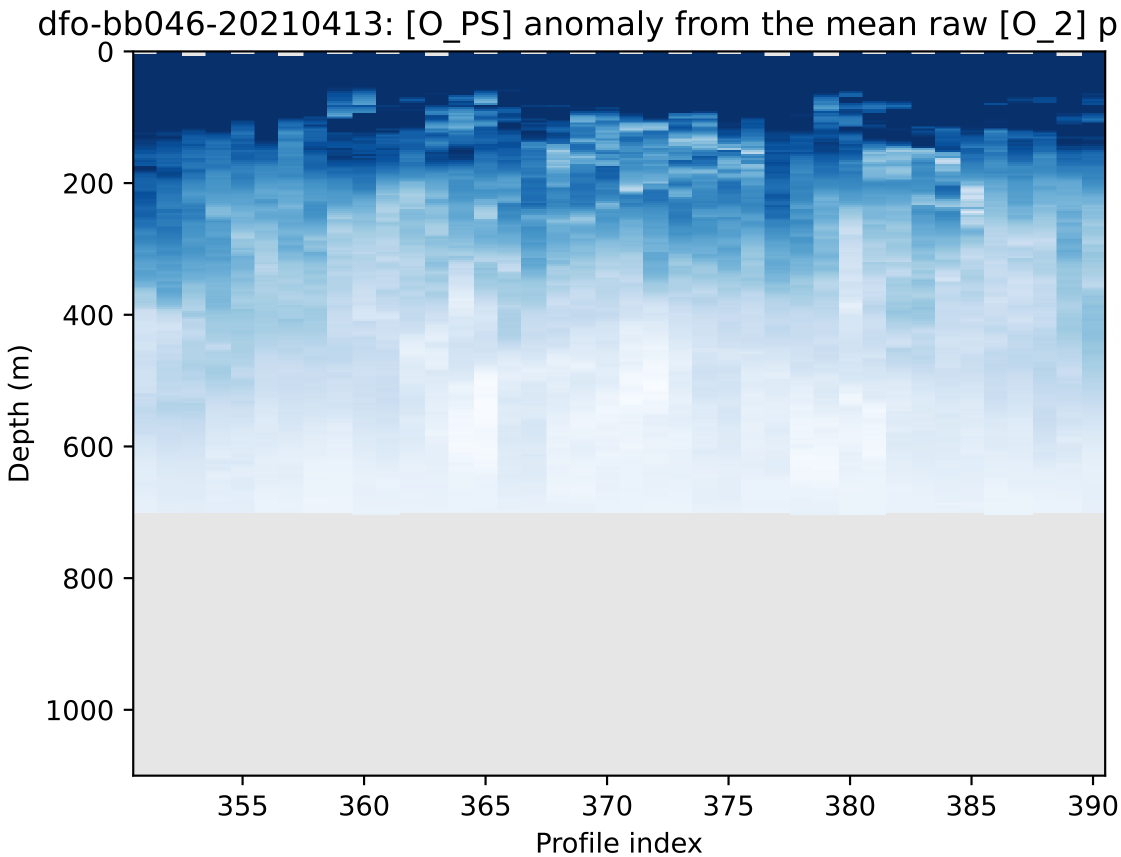

Figure 22: Example using dfo-bb046-20210413 with an Rinko O2 sensor: [O_2,PS] in depth space for profiles 350-390.

6 Optode drift

Over time, the luminophore foil degrades through exposure to light,sing optode measurements to drift toward lower oxygen concentrations relative to the true environmental conditions [Aanderaa Data Instruments AS, 2024]. A *drift correction* is therefore required to adjust the magnitude of $[O_2]$ to better represent the true oxygen concentration. Drift is often greatest early in the sensor's lifetime and subsequently approaches a more stable rate, such that changes between consecutive missions may be small relative to the uncertainty in the correction.

Both Aanderaa and Rinko optodes undergo a "burn-in" period, during which the sensor is run until there is a consistent drift with time [JFE Advantech Co., Ltd., 2023, Tengberg and Hovdenes, 2014]. The luminophore degrades faster out of water, particularly when exposed to light and air. To reduce this exposure, the sensor foil is covered with a moist tissue while the instrument is in the laboratory. For Argo deployments lasting several years, measurable drift may occur during a single mission. In contrast, glider missions generally last only weeks to months, and no measurable within-mission drift is typically observed.

Sensor drift is corrected using a linear adjustment to the dissolved oxygen concentration:

$$\text{oxygen\_concentration\_adjusted} = m \cdot DO + b$$

where m is the multiplicative gain and b is the additive offset. A linear model is assumed because long-term optode drift is typically dominated by gradual changes in sensor sensitivity rather than nonlinear changes in the oxygen response.

The drift correction is applied after the oxygen measurements have been compensated for pressure and salinity effects (Section 2) and corrected for sensor response time (Section 5). The same general procedure is used for both Aanderaa and Rinko optodes.

The sensor drift correction is applied to $[O_\tau]$ data that has been compensated for pressure-salinity effects (Section 2) and corrected for a time lag (Section 5). The same general procedure is used for both Aanderaa and Rinko optodes.

The gain and offset are determined by comparing the corrected glider oxygen observations with a trusted reference profile. Ideally, the reference consists of Winkler titrated bottle samples collected concurrently with a glider dive or a profile collected with an oxygen sensor that is regularly calibrated by comparison with Winkler titrations. When these measurements are unavailable, a hierarchy of alternative reference datasets collected by the Canadian government or the C-PROOF team during deployment or recovery is used. C-PROOF has also experimented with collecting in-air measurements while the glider is at the surface. These measurements have not yet been fully evaluated but may provide an additional reference for future calibrations.

Acceptable spatial and temporal separation depends on the study region and its oceanographic variability. For example, Line P extends approximately 1400 km offshore where water masses below the mixed layer evolve relatively slowly, allowing for more flexibility in how recent a profile needs to be to provide a reliable reference for calibration. The Queen Charlotte Sound Line (also referred to as the Calvert Line) is highly variable along the wide shelf region, making profiles collected more than a day apart unreliable for calibration. The suitability of a comparison profile should therefore be assessed to ensure that both observations sampled the same water mass before estimating sensor drift.

Physically, optode degradation is not expected to reverse with time. However, drift estimates from consecutive missions using the same sensor may occasionally indicate a smaller gain or offset for the later mission. These differences are interpreted as being within the uncertainty associated with the reference profile and the drift-fitting procedure rather than as evidence that the sensor recovered. We therefore apply the best available mission-specific drift correction, even when the estimated magnitude of the correction is smaller than that obtained for the preceding mission.

The drift-correction procedure depends on (1) whether a suitable reference profile is available and (2) whether previous drift estimates exist for the same optode. We use the *best* comparison data to calibrate the optode drift for a given mission.

1. Winkler-titrated bottle samples or a profile collected using an oxygen sensor that is regularly calibrated against Winkler titrations and sampled sufficiently close to the glider in space and time.

2. World Ocean Atlas data from well-sampled locations with a small standard deviation, such as 49.5°N, 134.5°W near station P16 and 49.5°N, 144.5°W near Ocean Station Papa. These locations are near regularly sampled Line P stations and are sufficiently far offshore to include contributions from Argo observations. This comparison is only considered valid when the glider travels sufficiently far offshore, approximately west of 134°W.
3. A gain and offset previously estimated for the same optode using a trusted comparison profile from another mission.
4. No drift correction is applied, and the absence of a suitable calibration reference is documented in the metadata.

The following sections describe several scenarios for applying the drift correction.

6.1 Scenario: A nearby calibrated CTD is available

walle)

6.1.1 Assemble and evaluate comparison CTD casts

Comparison CTD profiles collected by the Institute of Ocean Sciences (IOS), Fisheries and Oceans Canada, are considered reliable because the oxygen measurements are calibrated and corrected for sensor drift using Winkler titrations prior to publication. These can be accessed at `https://www.waterproperties.ca/data/`.

Mission dfo-walle652-20191209 coincided with an IOS Line P cruise (Figure 23a), a 1400 km hydrographic transect extending offshore from Vancouver Island. As a result, two deep CTD casts were available for comparison with nearby glider profiles (Figure 23b,c).

Although two high-quality comparison CTDs are available for this mission, the decadal mean World Ocean Atlas (WOA) profile at 49.5°N, 134.5°W is also included to evaluate whether climatological oxygen observations can provide a suitable substitute when comparison CTDs are unavailable. This grid cell is well-constrained in World Ocean Atlas by observations from repeated IOS Line P cruises and there is low oxygen variability below approximately 250 m suggesting that there is little seasonality at these depths. Consequently, this example provides an opportunity to assess the performance of a WOA-based drift correction against corrections derived from nearby calibrated CTD profiles.

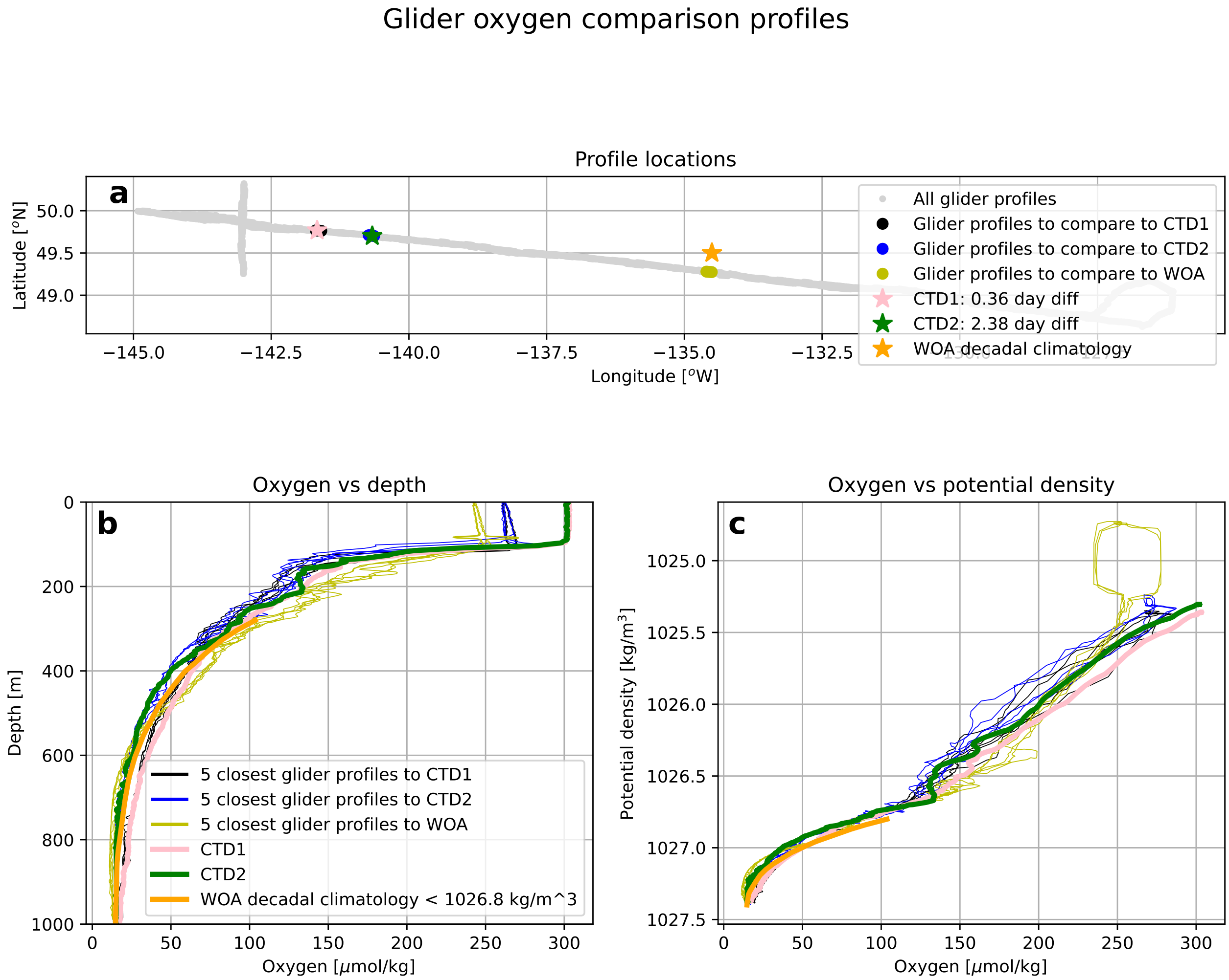

Figure 23: (a) Location of glider during the entire mission (gray), 5 closest glider profiles in time and space to CTD1 (black), and 5 closest glider profiles in time and space to CTD2 (blue). CTD1 and CTD2 collected by the Institute of Ocean Sciences, Department of Fisheries and Oceans, Canada are in pink and green respectively. In orange is the mean decadal World Ocean Atlas at 49.5N, 134.5W. In yellow are the 5 closest points in space to the WOA data used for comparison. (b) Oxygen vs. depth plots for 5 closest glider profiles in time and space to CTD1 (black), 5 closest glider profiles in time and space to CTD2 (blue), CTD1 (pink) and CTD2 (green), the 5 closest glider profiles in space to the WOA (yellow), and the WOA (orange) (c) Oxygen vs. potential density for 5 closest glider profiles in time and space to CTD1 (black), 5 closest glider profiles in time and space to CTD2 (blue), CTD1 (pink) and CTD2 (green), the 5 closest glider profiles in space to the WOA (yellow), and the WOA (orange).

6.1.2 Select glider profiles and assess the depth range to compare

Glider profiles selected for the drift correction should first be evaluated to ensure they sampled the same water mass as the comparison CTD. This assessment is performed by comparing temperature and temperature anomalies in density space (Figure 24a–f). Profiles exhibiting substantially different temperature structure or anomalies are excluded from the drift estimation because they likely sampled different water masses.

For example, profile 1236 has colder water between 1026 and 1026.5 kg m^{-3} than both the comparison CTD and the neighbouring glider profiles (Figure 24a,d), indicating that it sampled a different water mass. This profile was therefore excluded from the drift correction.

The second comparison CTD was collected approximately 2.3 days before the nearby glider profiles (Figure 24b,e), so fewer glider profiles are expected to sample the same water mass. Profiles 1274 and 1275 closely follow the temperature structure of the comparison CTD and remain within 0.2°C of the comparison (gray reference line), whereas the remaining profiles do not and were excluded.

The World Ocean Atlas (WOA) profile does not reproduce the observed water-mass properties above approximately 1026.3 kg m^{-3} (Figure 24c,f,i). Consequently, only observations denser than 1026.3 kg m^{-3} were included in the WOA comparison.

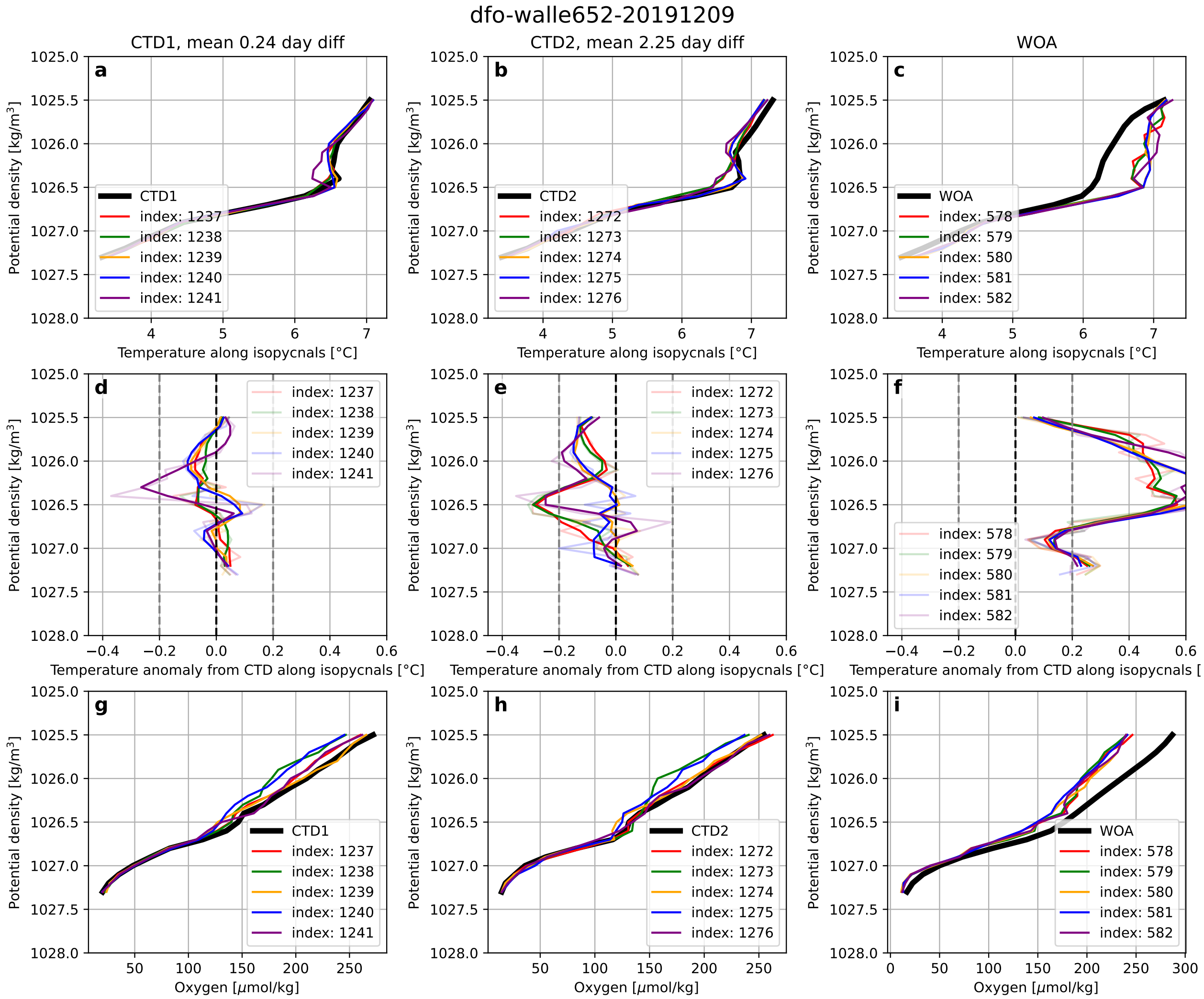

Figure 24: Temperature along isopycnals from the comparison (a) CTD1, (b) CTD2, and (c) World Ocean Atlas decadal climatology in black vs closest glider profile in time and space (orange) and 2 profiles before and after. (d-f) Temperature anomalies from comparison CTD along isopycnals. Light colours have a 0.1 kg/m^3 resolution and in dark colours are the results of a moving average over 3 points (0.3 kg/m^3) was applied. The light gray line represents -0.2C anomalies from the comparison CTD. (g-i) O2 along isopycnals from the comparison CTD (black) vs closest glider profile in time and space(orange) and 2 profiles before and after.

6.1.3 Density vs semi-Lagrangian depth bins

Several approaches for estimating the gain and offset were evaluated.

Map O_2 onto density surfaces

To minimize variability associated with isopycnal heave, glider and comparison CTD oxygen profiles sampling the same water mass were interpolated onto evenly spaced density surfaces between 1025.5 and 1028.5 kg m^{-3} at 0.04 kg m^{-3} intervals (Figure 25d-f). The density range and spacing were selected so that the homogeneous mixed-layer oxygen observations from both the glider and comparison CTD were represented within the same density bins while retaining sufficient resolution below the mixed layer. Because the raw glider observations systematically underestimate near-surface oxygen relative to the calibrated CTDs, ensuring a robust surface fit was a primary objective of the drift correction. For the WOA comparison, only observations denser than 1026.3 kg m^{-3} were included because shallower density surfaces did not represent the same water masses.

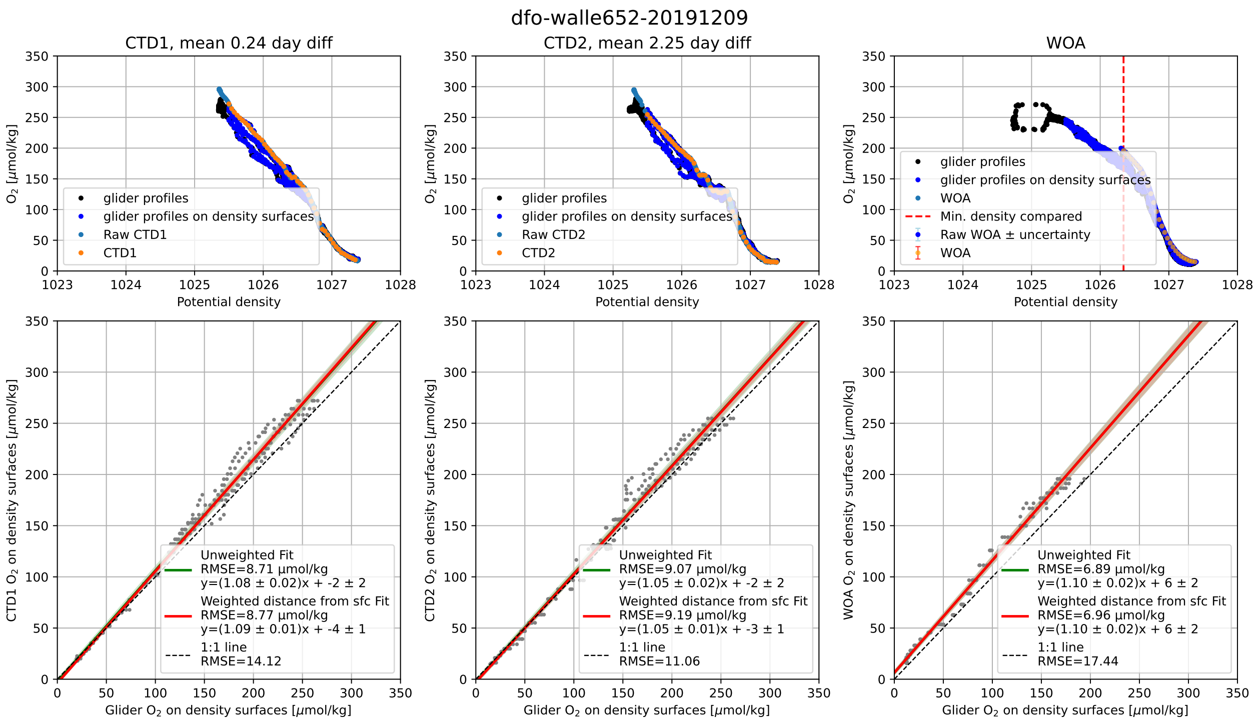

Figure 25: (a-c) Glider oxygen profiles compensated for pressure and salinity and adjusted for comparison CTD profiles (a,b) from the Institute of Ocean Sciences and the (c) World Ocean Atlas at 49.5N, 134.5W and glider profiles close in time and space sampling the same water masses (black). The dashed red line represents the upper limit of the WOA comparison at 1026.3 kg/m^3, the density water properties diverge. Glider oxygen profiles mapped onto density surfaces from 1025.5-1028.5 kg/m^3 with 0.04 kg/m^3 spacing. (d-f) Mean glider vs comparison CTD O_2 on density bins (gray). One-to-one line (dashed black). An unweighted linear regression of mean glider vs comparison CTD O_2 is plotted in green with 95% confidence intervals shaded (green). A linear regression of mean glider vs comparison CTD O_2 weighted by distance from the surface (red). The linear regression relating the glider and comparison O_2 are labelled with 95% uncertainty confidence intervals. Root mean square error (RMSE) for the unweighted, weighted and raw 1:1 comparison are included in the legend.

The estimated gain and offset are consistent, within their uncertainties, for both comparison CTDs (Figure 26g–i). Relative to the uncorrected glider observations, both the weighted and unweighted regressions reduce the root-mean-square error (RMSE) by more than 2 μmol/kg for CTD1, demonstrating that a drift correction is warranted. Because the unweighted regression provides the lowest RMSE while requiring fewer assumptions, it was selected as the preferred approach.

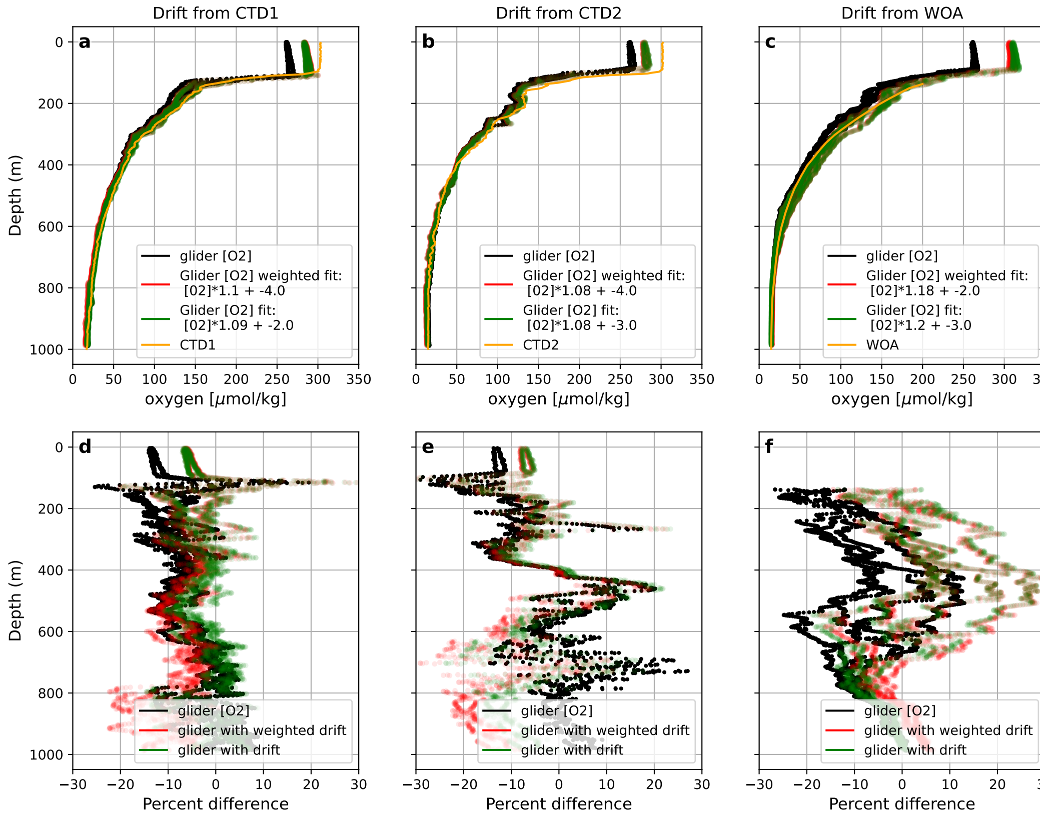

Figure 26: (a-c) Glider [O_2] profiles close in time and space to a comparison profiles: CTD1 (a) and CTD2 (b)from the Institute of Ocean Sciences, and the World Ocean Atlas at 49.5N, 134.5W (c). Glider [O_2] is plotted without a drift correction (black), and with a gain and offset found using a linear re.g,ression weighted by distance from the surface (red), and with a gain and offset found using an unweighted linear re.g,ression (green). Comparison profiles are in orange.(d-f) Percent difference of raw (black), with a gain and offset found using a linear re.g,ression weighted by distance from the surface (red) and with a gain and offset found using an unweighted linear re.g,ression (green).

The estimated gain and offset depend on the choice of density-bin spacing. A resolution of 0.04 kg m^{-3} was selected because it places the homogeneous mixed-layer oxygen observations from both the comparison CTD and the glider into comparable density bins while retaining a large number of near-surface observations in the regression (Figure 25g-i). Accurately correcting near-surface oxygen was a primary objective because the largest differences between the glider and comparison CTD occur in the upper water column.

Both weighted and unweighted linear regressions were evaluated. Weighting the regression toward near-surface observations did not improve the correction relative to the unweighted fit. For CTD1, the closest comparison profile in time and space, the unweighted regression provided the best agreement throughout the water column, including near the surface (Figure 26d). For CTD2, collected approximately two days earlier, the weighted and unweighted regressions produced similar results (Figure 26e).

Using the WOA below 1026.3 kg m^{-3} produced oxygen concentrations at depth comparable to those obtained using the comparison CTDs (Figure 26c), suggesting that WOA can provide a reasonable substitute for a comparison CTD in offshore regions where deep-water properties evolve slowly. The final oxygen product obtained using the unweighted regression with CTD1 is shown in Figure 1d.

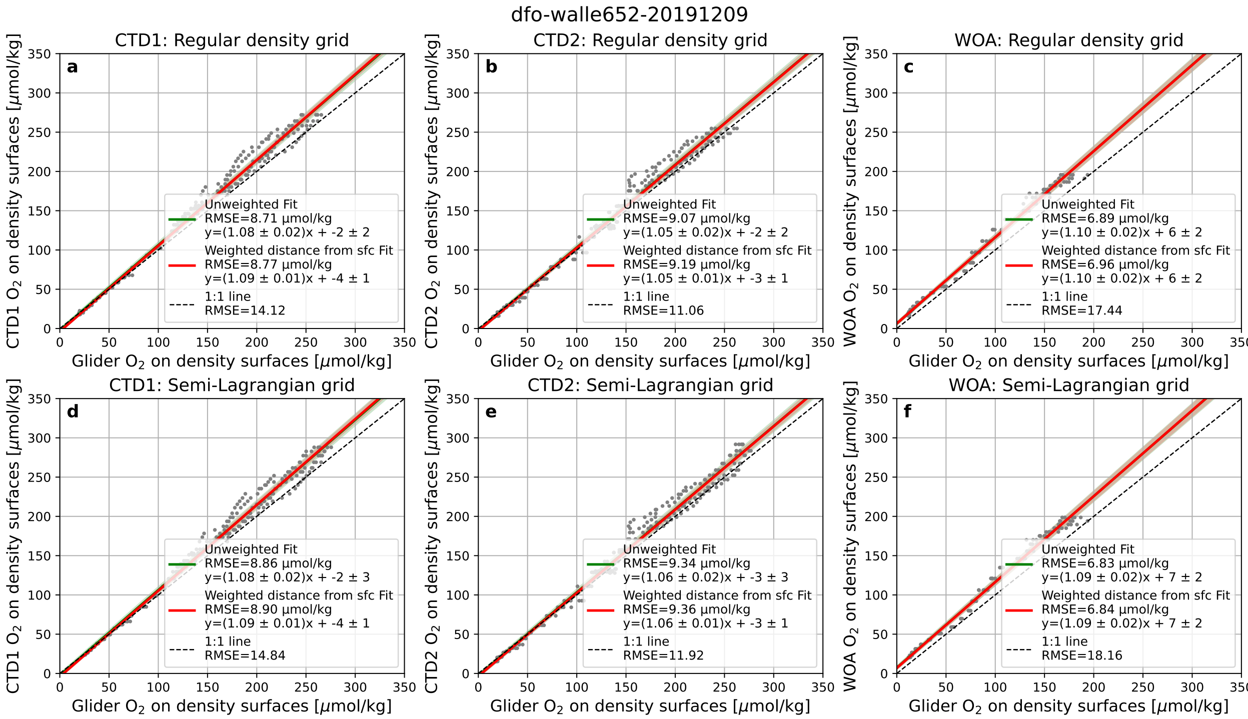

Figure 27: Comparison of glider dissolved oxygen interpolated onto density surfaces with three reference datasets for mission dfo-walle652-20191209. (a–c) Comparisons using interpolation onto a regular potential-density grid. (d–f) Comparisons using interpolation onto the semi-Lagrangian density grid described by Talbot et al. (2026). Columns show comparisons with (a,d) CTD1, (b,e) CTD2, and (c,f) World Ocean Atlas (WOA) at 49.5N, 134.5W. Gray points show paired glider and reference oxygen values, the dashed black line is the 1:1 relationship, the green line is the unweighted linear regression, and the red line is the regression weighted by distance from the sea surface. The root-mean-square error (RMSE) and fitted regression equations are reported for each comparison.

Although multiple comparison profiles can be combined into a weighted average, using the closest calibrated CTD in space and time provided the most robust and simplest correction. Combining CTD1, CTD2, and the WOA did not improve the agreement and introduced additional uncertainty.

Recommendation: Use the closest calibrated CTD profile in space and time to estimate the gain and offset. An unweighted linear regression provides the preferred drift correction.

Map O_2 onto semi-lagrangian density surfaces

Semi-Lagrangian density surfaces, defined as the mean isopycnal depth for this region by Talbot et al., were also evaluated as an alternative to fixed density surfaces. Because these surfaces are more closely spaced near the surface, they effectively place greater weight on the upper ocean, where the largest oxygen differences between the glider and comparison profiles occur (Figure 27).

However, the estimated gain and offset were indistinguishable, within uncertainty, from those obtained using fixed density surfaces. Consequently, mapping oxygen onto semi-Lagrangian density surfaces did not improve the drift correction sufficiently to justify the additional computational effort.

6.2 Scenario: A shallow deployment CTD is available.

Some missions exhibit little evidence of sensor drift because the corrected glider oxygen observations already agree closely with an independent comparison profile. An example is dfo-hal1002-20240924, for which a CTD cast was collected by the C-PROOF team during deployment in Queen Charlotte Sound (QCS; Figure 28a). Only the glider upcasts (even-numbered profiles) were used for comparison because they sampled water masses most consistent with the deployment CTD (Figures 28b,c and 29e). Downcasts were excluded because QCS is a highly dynamic environment, and organic material may have temporarily fouled the optode, producing systematic differences during descent.

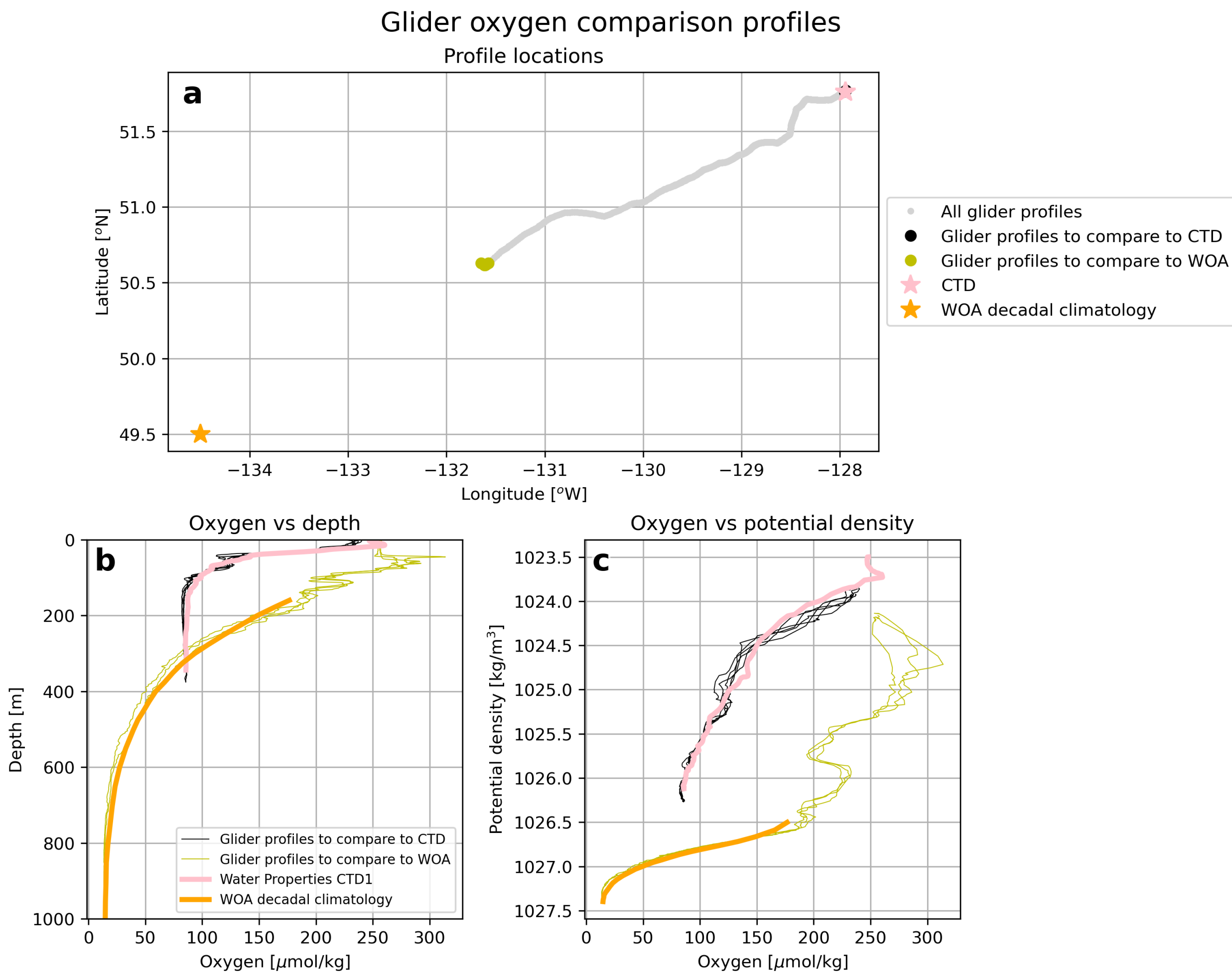

Figure 28: (a) Location of glider during the entire mission (gray), 5 closest glider profiles in time and space to the comparison CTD (black) collected by the C-PROOF team at deployment. In orange is the mean decadal World Ocean Atlas (WOA) at 49.5N, 134.5W. In yellow are the 5 closest points in space to the WOA data used for comparison. (b) Oxygen vs. depth plots for 5 closest glider profiles in time and space to the comparison CTD (black), the CTD (pink), the 5 closest glider profiles in space to the WOA (yellow), and the WOA (orange). (c) Oxygen vs. potential density for the 5 closest glider profiles in time and space to the comparison CTD (black), the CTD (pink), the 5 closest glider profiles in space to the WOA (yellow), and the WOA (orange).

Fitting a linear gain and offset to the deployment CTD changed the root-mean-square error (RMSE) by less than 2 μmol/kg, indicating that the pressure-, salinity-, and time-response-corrected oxygen observations already agree closely with the CTD (Figure 30a,c,e). Because the RMSE is integrated over the full depth range, however, a 2 μmol/kg difference can still be important at depth, where natural oxygen gradients are

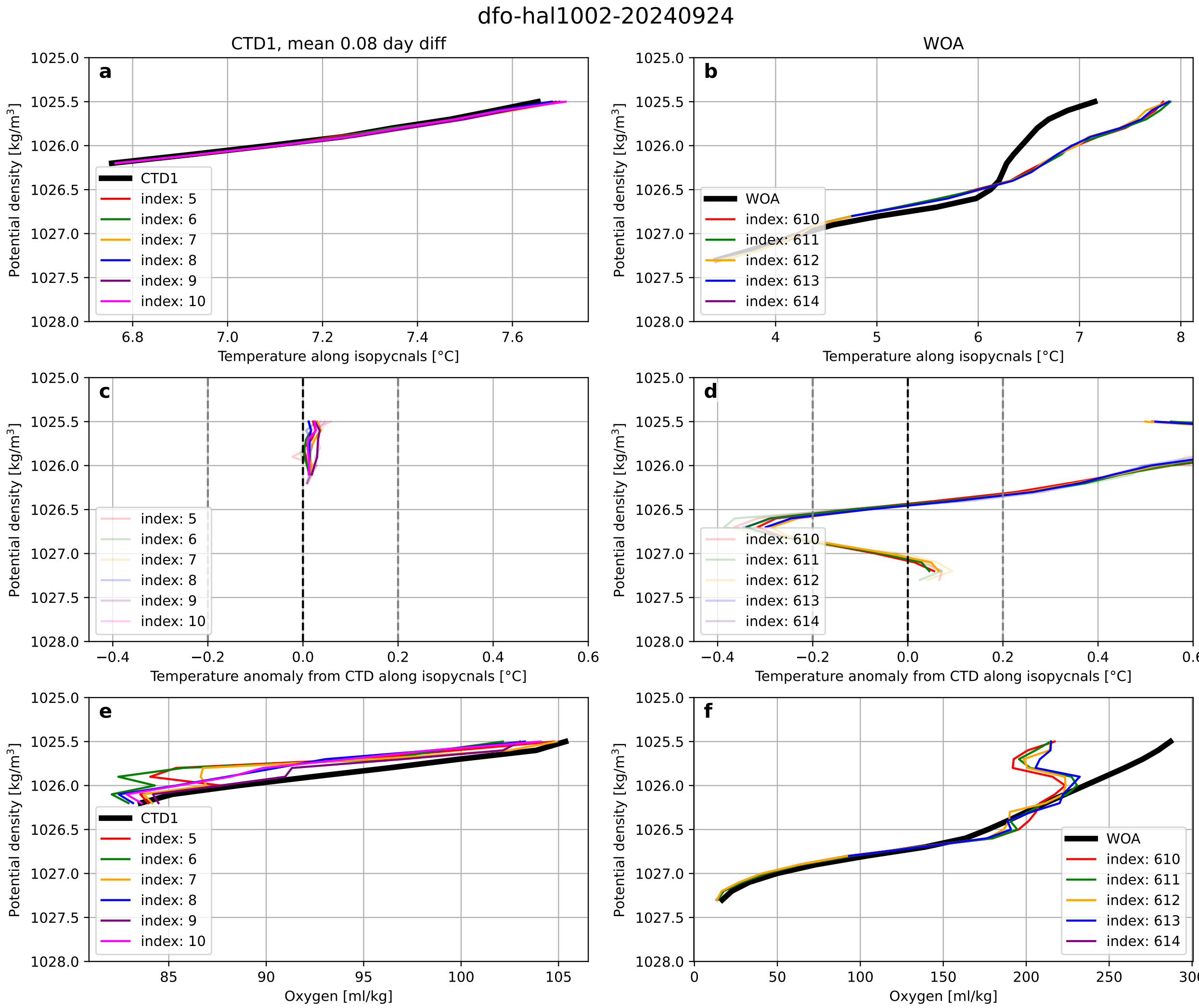

Figure 29: Temperature along isopycnals from the comparison (a) CTD and (b) World Ocean Atlas decadal climatology in black vs closest glider profile in time and space (orange) and 2 profiles before and after. (c,d) Temperature anomalies from comparison CTD and WOA along isopycnals. Light colours have a 0.1 kg/m^3 resolution and in dark colours are the results of a moving average over 3 points (0.3 kg/m^3) was applied. The light gray line represents -0.2C anomalies from the comparison profile. (e,f) O2 along isopycnals from the comparison CTD (black) vs closest glider profile in time and space and 2 profiles before and after.

relatively weak.

To better constrain the lower oxygen concentrations that were not sampled by the deployment CTD, we also evaluated a combined fit using both the deployment CTD and the World Ocean Atlas (WOA) comparison profiles (Figures 28b,c and 31). This combined fit also changed the RMSE by less than 2 μmol/kg, further supporting the conclusion that the optode exhibited negligible drift during the mission.

The processing sequence for this mission is shown in Figure 32. Because no measurable drift was detected, the final oxygen product is identical to the pressure-, salinity-, and time-response-corrected oxygen concentration.

Recommendation: A drift correction should not be applied when fitting the gain and offset changes the RMSE by less than 2 μmol/kg.

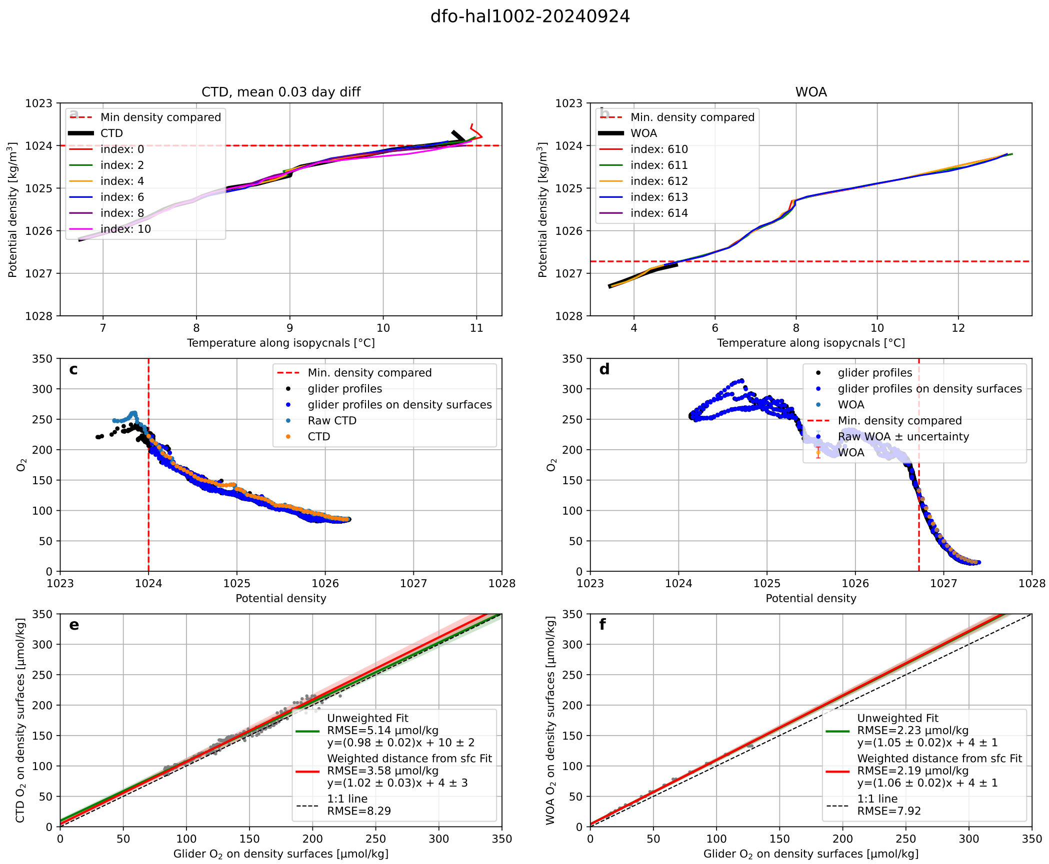

Figure 30: Temperature along isopycnals for comparison CTD profiles (a) from the Institute of Ocean Sciences and the (b) World Ocean Atlas at 49.5N, 134.5W and glider profiles close in time and space sampling the same water masses. The dashed red line represents the upper limit of the CTD comparsion (1025 kg/m^3) and the WOA comparison (1026.3 kg/m^3) where the density water properties diverge.(c,d) Glider oxygen profiles compensated for pressure and salinity and adjusted for time response close in time and space sampling the same water masses as comparison profiles (black). Glider oxygen profiles mapped onto density surfaces from 1025.5-1028.5 kg/m^3 with 0.04 kg/m^3 spacing. The dashed red line in (f) represents the upper limit of the CTD and WOA comparisons. (e,f) Mean glider vs comparison O_2 profile on density bins (gray). One-to-one line (dashed black). An unweighted linear regression of mean glider vs comparison CTD O_2 is plotted in green with 95% confidence intervals shaded (green). A linear regression of mean glider vs comparison O_2 profile weighted by distance from the surface (red). The linear regression relating the glider and comparison O_2 are labelled with 95% uncertainty confidence intervals.

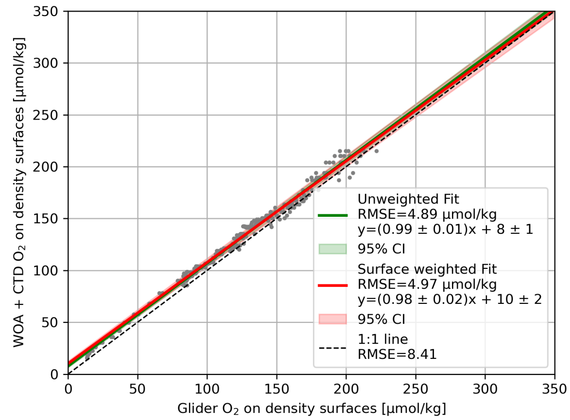

Figure 31: (a) Location of glider during the entire mission (gray) In orange is the mean decadal World Ocean Atlas (WOA) at 49.5N, 134.5W. In yellow are the 5 closest points in space to the WOA data used for comparison. (b) Oxygen vs. depth plots the 5 closest glider profiles in space to the WOA (yellow), and the WOA (orange). (c) Oxygen vs. potential density for the 5 closest glider profiles in space to the WOA (yellow), and the WOA (orange).

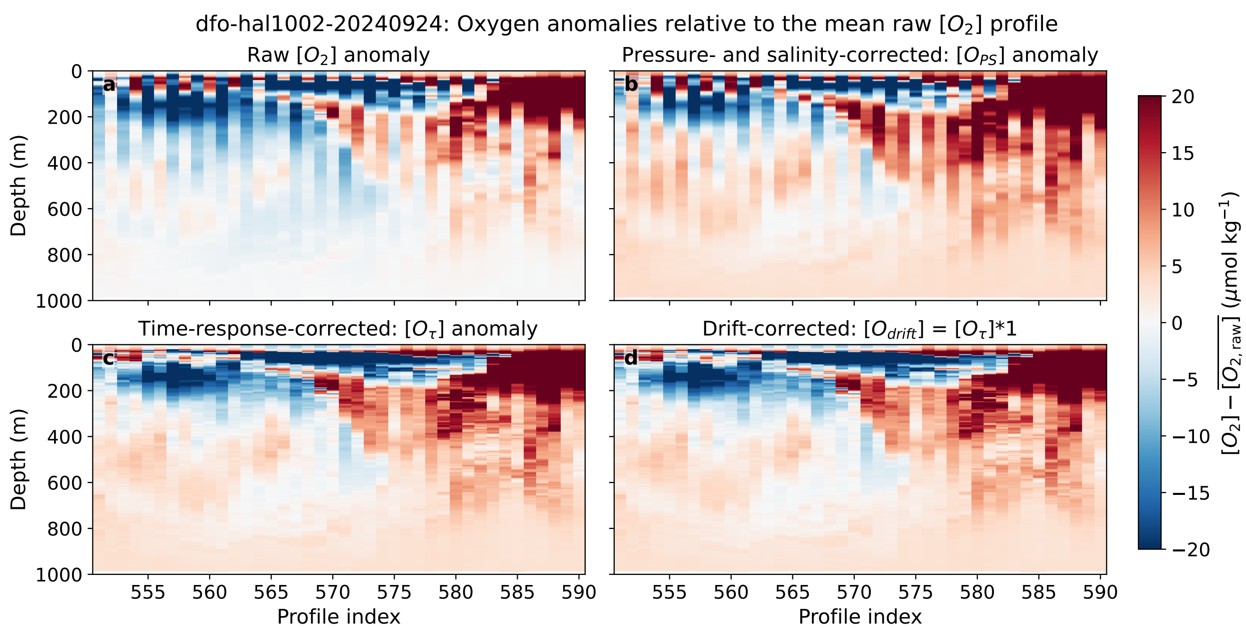

Figure 32: Example using dfo-hal1002-20240924 with Aanderaa optode 4381: (a) Raw oxygen concentration ($[O_2]$) collected by the optode, (b) Raw $[O_2]$ accounting for pressure and salinity effects (PS effects), (c) $[O_2]$ accounting for PS effects and sensor response time, (d) equivalent to $[O_2]$ from (c) since no drift correction is needed.

6.3 Scenario: No CTD is available but the mission extends offshore.

Some missions were collected during gaps in cruises and no CTD was taken at deployment or recovery. For offshore missions extending beyond approximately 128°W, the World Ocean Atlas (WOA) profile at Line P is generally consistent with observed glider water masses. As demonstrated above, gain and offset estimates derived from the WOA below the density threshold produce drift corrections comparable to those obtained using calibrated CTD profiles(Figures 25/30).

For example, oxygen observations from dfo-rosie713-20240501 agree well with the Line P WOA profile below 1026.7 kg m^{-3}. A gain of 1.14 and an offset of (-2) μmol/kg were estimated from the WOA comparison, increasing near-surface oxygen concentrations to values comparable with those from other drift-corrected missions in the region (Figure 26/1). Although calibrated CTD profiles remain the preferred reference for estimating sensor drift, these results indicate that the WOA provides a suitable alternative for offshore missions where no comparison CTD is available.

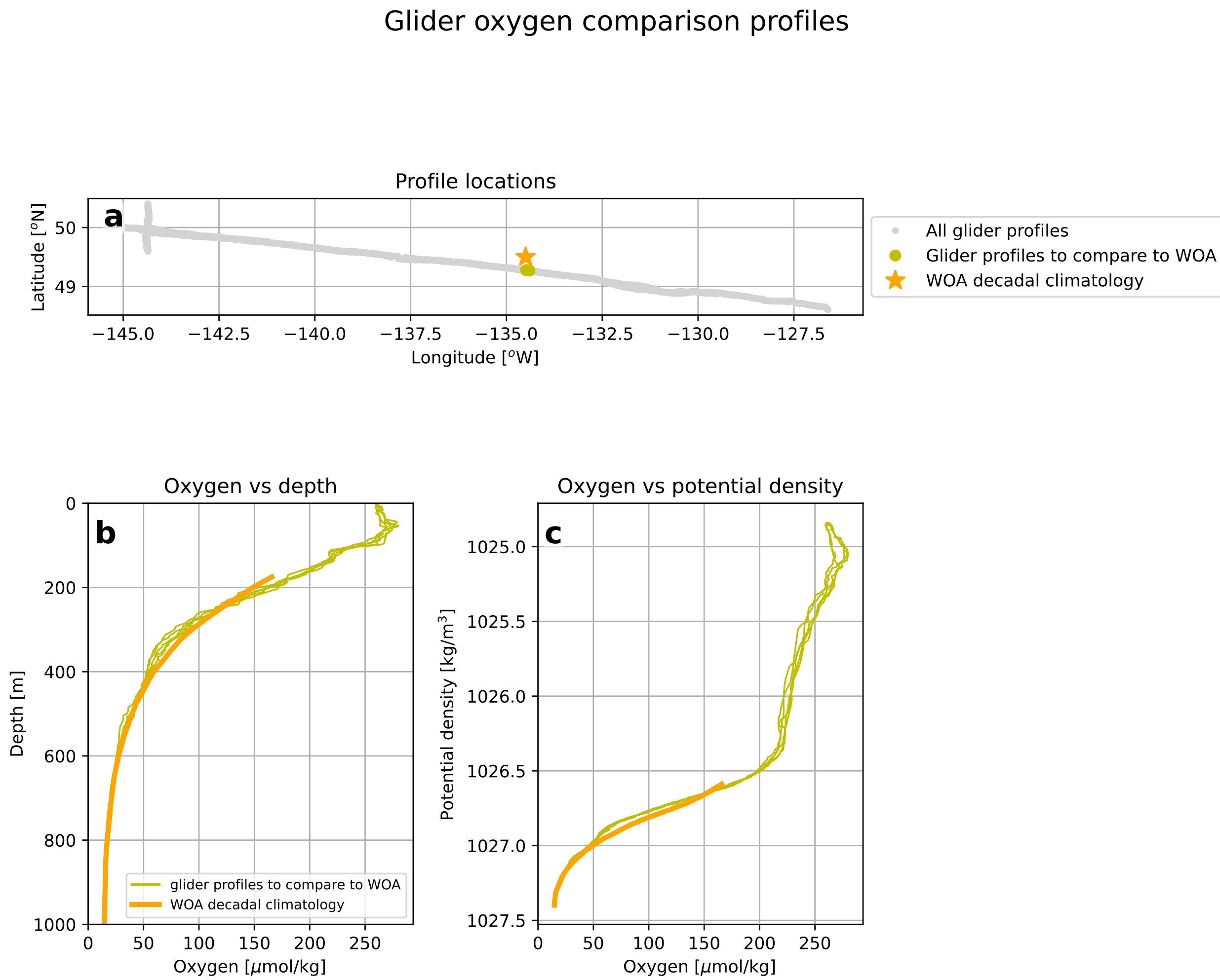

Figure 33: Example of the combined-reference drift correction for mission dfo-hal1002-20240924. Oxygen concentrations interpolated onto density surfaces from the glider are compared with a reference profile created by merging CTD observations in the upper water column with WOA observations at depth. The combined dataset constrains the gain and offset over the entire profile, allowing a single linear drift correction to be estimated. The dashed line indicates the 1:1 relationship, and the green and red lines show the unweighted and surface-weighted regressions with 95% confidence intervals.

Recommendation: WOA may be used below the density threshold when no suitable CTD profile is

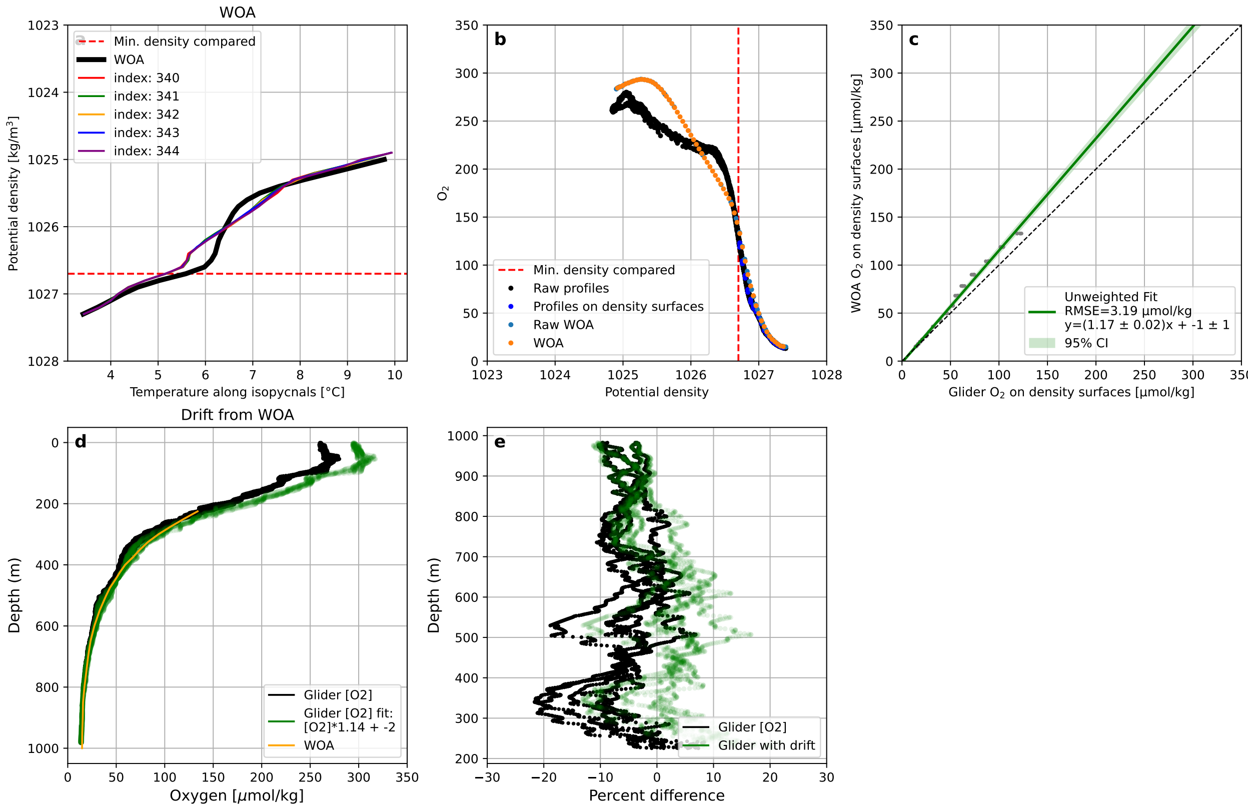

Figure 34: (a) Temperature along isopycnals for comparison World Ocean Atlas at 49.5N, 134.5W and glider profiles close in space sampling the same water masses. The dashed red line represents the upper limit of the WOA comparison (1026.7 kg/m^3) where the density water properties diverge.(b) Glider oxygen profiles compensated for pressure and salinity and adjusted for time response close in time and space sampling the same water masses as comparison profiles (black). Glider oxygen profiles mapped onto density surfaces from 1025.5-1028.5 kg/m^3 with 0.04 kg/m^3 spacing. The dashed red line represents the upper limit of the comparison. (c) Mean glider vs WOA comparison O_2 profile on density bins (gray). One-to-one line (dashed black). An unweighted linear re.g,ression of mean glider vs comparison WOA O_2 is plotted in green with 95% confidence intervals shaded (green). A linear re.g,ression of mean glider vs comparison O_2 profile weighted by distance from the surface (red). The linear re.g,ression relating the glider and comparison O_2 are labelled with 95% uncertainty confidence intervals. (d) Glider [O_2] profiles close space to the World Ocean Atlas at 49.5N, 134.5W plotted without a drift correction (black), and with a gain and offset found using an unweighted linear re.g,ression (green). The comparison WOA profile are in orange.(e) Percent difference of raw (black) with a gain and offset found using an unweighted linear re.g,ression (green).

available.

6.4 Senario: No CTD is available and the mission is close to shore

There are missions for which no suitable comparison CTD is available to estimate sensor drift. Because oxygen optodes typically drift slowly and C-PROOF observations indicate that drift remains relatively consistent through time for a given sensor, the preferred approach is to apply the gain and offset estimated from the closest mission for the same optode that has a trusted comparison profile. If no such mission exists, the World Ocean Atlas (WOA) should be evaluated as an alternative reference.

The WOA provides a suitable reference only for missions extending sufficiently far offshore, where deep-water properties remain relatively stable through time. In contrast, waters over the continental shelf are highly variable, resulting in larger WOA standard deviations and fewer observations contributing to the climatological mean (Figure 35). Consequently, WOA comparisons are most reliable near frequently occupied Line P stations where repeated hydrographic observations contribute to the climatology.

Mission dfo-bumblebee998-20221207 provides an example where the WOA is not a suitable substitute (Figure 36). The offshore WOA profile that performs well for other Line P missions (Section ??) is located too far from the glider track (Figure 36a), and its deep oxygen concentrations are inconsistent with the observed glider profiles (Figure 36b,c). A second, nearer WOA profile contains sufficient observations (N = 187, ($\alpha = 1.3$); Figure 35) and agrees reasonably well with the glider below approximately 650 m (1027.2 kg m^{-3}; Figures 36b,c/37c,d). However, the comparison spans too small a density range to constrain a reliable linear gain and offset (Figure 37e,f). In this case, a drift correction cannot be justified, and the absence of a drift correction should be documented in the mission metadata.

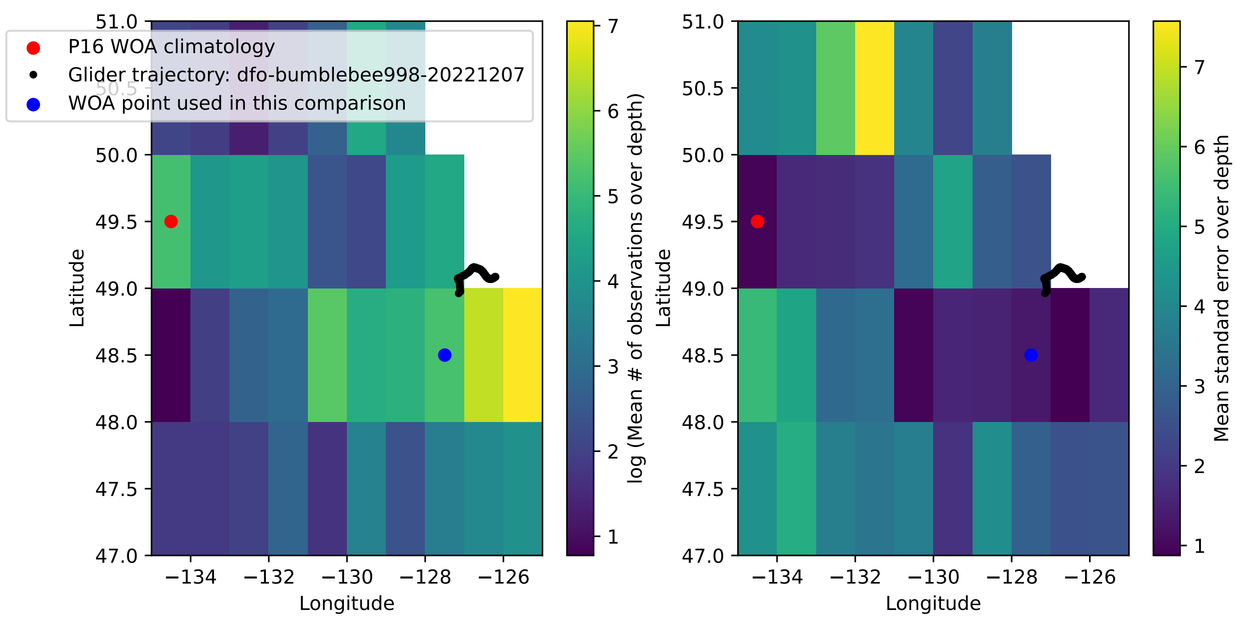

Figure 35: (a) Log scale of mean number of oxygen observations in the WOA decadal climatology averaged with depth. The black line is the glider trajectory for dfo-bumblebee998-20221207. The red dot is the WOA climatology that includes P16 data. The blue dot is the another WOA data point with 187 points and a standard deviation of 1.3, located off the continental shelf. (b) Log scale of the standard deviation of oxygen.

Recommendation: If neither a trusted comparison CTD, a previous calibration for the same optode, nor a suitable WOA comparison is available, no drift correction should be applied. The lack of a drift correction should be recorded in the metadata.

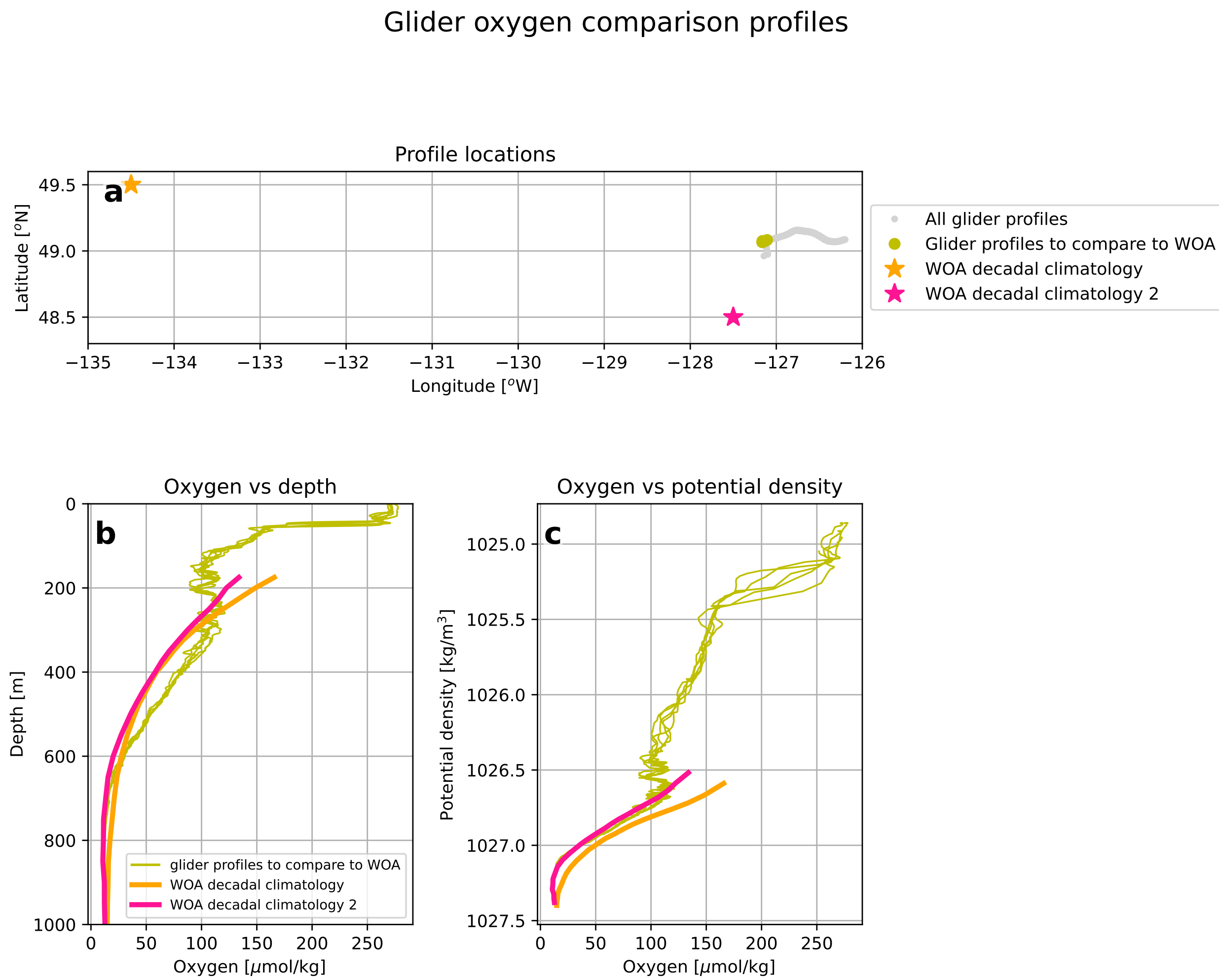

Figure 36: (a) Location of glider during the entire mission (gray) In orange is the mean decadal World Ocean Atlas (WOA) at 49.5N, 134.5W and in pink is the mean decadal World Ocean Atlas (WOA) at 48.5N, 127.5W, reffered to as WOA 2. In yellow are the 5 closest points in space to the WOA data used for comparison. (b) Oxygen vs. depth plots the 5 closest glider profiles in space to the WOA (yellow), the WOA (orange), and WOA 2 (pink). (c) Oxygen vs. potential density for the 5 closest glider profiles in space to the WOA (yellow), the WOA (orange), and WOA 2 (pink).

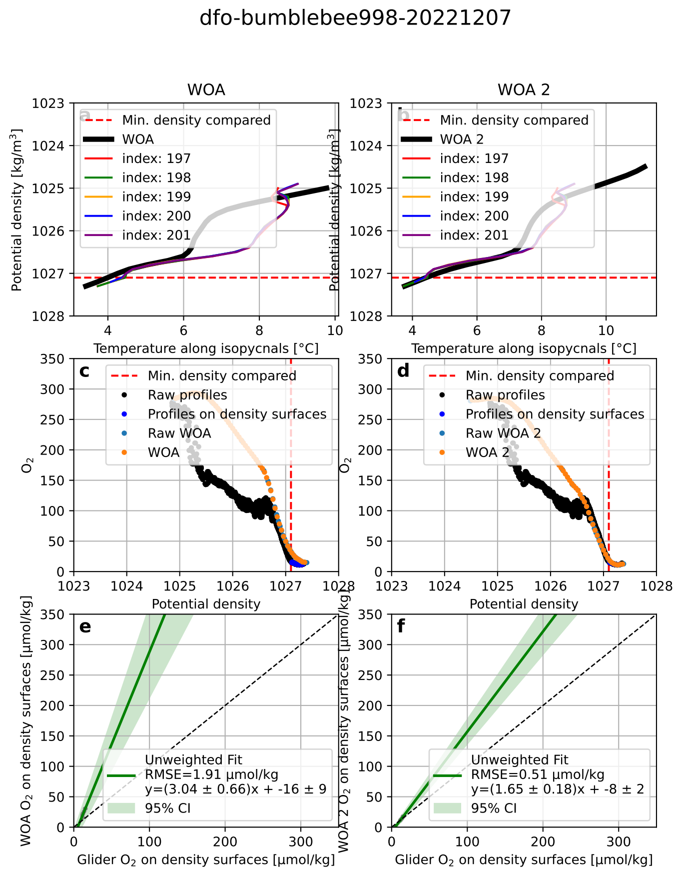

Figure 37: Temperature along isopycnals for the World Ocean Atlas at 49.5N, 134.5W and glider profiles close in space, sampling the same water masses. The dashed red line represents the upper limit of the WOA comparison (1026.3 kg/m^3) where the density water properties diverge.(c,d) Glider oxygen profiles compensated for pressure and salinity and adjusted for time response close in space, sampling the same water masses as comparison WOA profile (black). Glider oxygen profiles mapped onto density surfaces from 1025.5-1028.5 kg/m^3 with 0.04 kg/m^3 spacing. The dashed red line in (f) represents the upper limit of the WOA comparison. (e,f) Mean glider vs comparison WOA O_2 on density bins (gray). One-to-one line (dashed black). An unweighted linear re.g,ression of mean glider vs comparison WOA O_2 is plotted in green with 95% confidence intervals shaded (green). A linear re.g,ression of mean glider vs comparison WOA O_2 weighted by distance from the surface (red). The linear re.g,ression relating the glider and comparison O_2 are labelled with 95% uncertainty confidence intervals.

7 Conclusion

This document describes the delayed-mode oxygen processing methodology currently used by C-PROOF for Aanderaa 4831 and Rinko AROD-FT optodes. Oxygen observations are corrected sequentially for salinity and pressure effects, sensor response time, and long-term sensor drift.

For Aanderaa optodes, a single mission-specific response time provides a robust balance between computational efficiency and correction performance. More complex approaches, including two-regime and time-varying response times, were evaluated but did not produce sufficient improvement to justify their additional complexity. Rinko optodes generally require little or no response time correction because of their substantially faster sensor response.

Optode drift should be estimated using the highest-quality comparison data available. A nearby calibrated CTD profile is preferred whenever possible. When no suitable CTD is available, offshore World Ocean Atlas climatology may provide a reasonable alternative where deep water properties are stable. If no reliable comparison exists, no drift correction should be applied, and this decision should be documented in the metadata.

The procedures described here provide a consistent framework for delayed-mode oxygen processing while allowing users to adopt alternative methods if warranted by the scientific objectives of a particular mission.

References

Aanderaa Data Instruments AS. *TD 269 OPERATING MANUAL:OXYGEN OPTODE 4330, 4831, 4835*. Aanderaa Data Instruments AS, Nesttun, Norway, 7th edition, June 2017. Available at `https://www.aanderaa.com/media/pdfs/oxygen-optode-4330-4835-and-4831.pdf`.

Aanderaa Data Instruments AS. Aanderaa oxygen optodes: Quick reference selection guide. Technical Report XA F2024-F1, Xylem Inc., 2024. URL `https://www.aanderaa.com/media/pdfs/2024-f1-quick-reference-oxygen-optode-selection-guide.pdf`.

Henry C. Bittig, Björn Fiedler, Roland Scholz, Gerd Krahmann, and Arne Körtzinger. Time response of oxygen optodes on profiling platforms and its dependence on flow speed and temperature. *Limnology and Oceanography: Methods*, 12(8):617–636, 2014. doi: https://doi.org/10.4319/lom.2014.12.617. URL `https://aslopubs.onlinelibrary.wiley.com/doi/abs/10.4319/lom.2014.12.617`.

Henry C. Bittig, Arne Körtzinger, Craig Neill, Eikbert van Ooijen, Joshua N. Plant, Johannes Hahn, Kenneth S. Johnson, Bo Yang, and Steven R. Emerson. Oxygen optode sensors: Principle, characterization, calibration, and application in the ocean. *Frontiers in Marine Science*, Volume 4 - 2017, 2018. ISSN 2296-7745. doi: 10.3389/fmars.2017.00429. URL `https://www.frontiersin.org/journals/marine-science/articles/10.3389/fmars.2017.00429`.

N. P. Fofonoff, S. P. Hayes, and R. C. Millard. *W.H.O.I./Brown CTD Microprofiler : Methods of Calibration and Data Handling*. Woods Hole Oceanographic Institution, 1974. doi: 10.1575/1912/647. URL `https://hdl.handle.net/1912/647`.

A.A. Hare, W. Evans, H.V. Dosser, J.M. Jackson, S.R. Alin, C. Hannah, T. Ross, and J.M. Klymak. Regression-based characterization of the marine carbonate system across shelf and nearshore waters of Queen Charlotte Sound. 270:104511. ISSN 03044203. doi: 10.1016/j.marchem.2025.104511. URL `https://linkinghub.elsevier.com/retrieve/pii/S030442032500026X`.

JFE Advantech Co., Ltd. *Manual for ARO-FT Dissolved Oxygen Sensor*. JFE Advantech Co., Ltd., 2023. URL `https://www.jfe-advantech.co.jp/eng/ocean/rinko/`. English version.

David Nicholson, Steven Emerson, and Charles C. Eriksen. Net community production in the deep euphotic zone of the subtropical north pacific gyre from glider surveys. *Limnology and Oceanography*, 53(5part2):2226–2236, 2008. doi: https://doi.org/10.4319/lo.2008.53.5_part_2.2226. URL `https://aslopubs.onlinelibrary.wiley.com/doi/abs/10.4319/lo.2008.53.5_part_2.2226`.

Tetjana Ross, Hayley Dosser, Jody Klymak, Wiley Evans, Alex Hare, Jennifer Jackson, and Stephanie Waterman. Ocean Gliders for Planning and Monitoring Remote Canadian Pacific Marine Protected Areas. ISSN 10428275. doi: 10.5670/oceanog.2025e104. URL https://tos.org/oceanography/article/ocean-gliders-for-planning-and-monitoring-remote-canadian-pacific-marine-protected-areas.

S. W. Stevens, C. Hannah, W. Evans, J. Klymak, S. Waterman, and T. Ross. Dissolved Oxygen Variability on the Canadian Pacific Shelf: Trends, Drivers, and Projections in the Context of Emerging Hypoxia in Queen Charlotte Sound. 39(8):e2025GB008608. ISSN 0886-6236, 1944-9224. doi: 10.1029/2025GB008608. URL https://agupubs.onlinelibrary.wiley.com/doi/10.1029/2025GB008608.

Lauryn C. Talbot, Jody M. Klymak, Tetjana Ross, and Guoqi Han. Two Lateral Stirring Regimes in the Northeast Pacific. 131(3):e2025JC023699. ISSN 2169-9275, 2169-9291. doi: 10.1029/2025JC023699. URL https://agupubs.onlinelibrary.wiley.com/doi/10.1029/2025JC023699.

Anders Tengberg and Jostein Hovdenes. Information on long-term stability and accuracy of aanderaa oxygen optodes. Technical report, Aanderaa Data Instruments AS, April 2014. URL https://www.aanderaa.com/media/pdfs/2014-04-02-optode-and-calibration.pdf. Information on multipoint calibration system and sensor option overview.

Anders Tengberg, Jostein Hovdenes, Henrik Johan Andersson, Olivier Brocandel, Robert Diaz, David Hebert, Tony Arnerich, Christian Huber, Arne Körtzinger, Alexis Khripounoff, Francisco Rey, Christer Rönning, Jens Schimanski, Stefan Sommer, and Achim Stangelmayer. Evaluation of a lifetime-based optode to measure oxygen in aquatic systems. *Limnology and Oceanography: Methods*, 4(2):7–17, 2006. doi: https://doi.org/10.4319/lom.2006.4.7. URL https://aslopubs.onlinelibrary.wiley.com/doi/abs/10.4319/lom.2006.4.7.